The *lhfpl5* ohnologs *lhfpl5a* and *lhfpl5b* are required for mechanotransduction in distinct populations of sensory hair cells in zebrafish.

Timothy Erickson[1, 2*], Itallia V. Pacentine[2], Alexandra Venuto[1], Rachel Clemens[2], and Teresa Nicolson[2, 3]

[1] Department of Biology, East Carolina University, Greenville, NC, USA.

[2] Vollum Institute and Oregon Hearing Research Center, OHSU, Portland, OR, USA.

[3] Current address: Otolaryngology-Head & Neck Surgery, Stanford School of Medicine, Stanford, CA, USA

*** Correspondence:**
Dr. Timothy Erickson, Department of Biology, East Carolina University, Greenville, NC, USA.
ericksonti17@ecu.edu

Keywords: hair cell, mechanotransduction, deafness, lateral line, zebrafish, LHFPL5, TMC1, PCDH15

Article type

Original Research

1 Abstract

Hair cells sense and transmit auditory, vestibular, and hydrodynamic information by converting mechanical stimuli into electrical signals. This process of mechano-electrical transduction (MET) requires a mechanically-gated channel localized in the apical stereocilia of hair cells. In mice, lipoma HMGIC fusion partner-like 5 (LHFPL5) acts as an auxiliary subunit of the MET channel whose primary role is to correctly localize PCDH15 and TMC1 to the mechanotransduction complex. Zebrafish have two *lhfpl5* genes (*lhfpl5a* and *lhfpl5b*), but their individual contributions to MET channel assembly and function have not been analyzed.

Here we show that the zebrafish *lhfpl5* genes are expressed in discrete populations of hair cells: *lhfpl5a* expression is restricted to auditory and vestibular hair cells in the inner ear, while *lhfpl5b* expression is specific to hair cells of the lateral line organ. Consequently, *lhfpl5a* mutants exhibit defects in auditory and vestibular function, while disruption of *lhfpl5b* affects hair cells only in the lateral line neuromasts. In contrast to previous reports in mice, localization of Tmc1 does not depend upon Lhfpl5 function in either the inner ear or lateral line organ. In both *lhfpl5a* and *lhfpl5b* mutants, GFP-tagged Tmc1 and Tmc2b proteins still localize to the stereocilia of hair cells. Using a stably integrated GFP-Lhfpl5a transgene, we show that the tip link cadherins Pcdh15a and Cdh23, along with the Myo7aa motor protein, are required for correct Lhfpl5a localization at the tips of stereocilia. Our work corroborates the evolutionarily conserved co-dependence between Lhfpl5 and Pcdh15, but also reveals novel requirements for Cdh23 and Myo7aa to correctly localize Lhfpl5a. In addition, our data suggest that targeting of Tmc1 and Tmc2b proteins to stereocilia in zebrafish hair cells occurs independently of Lhfpl5 proteins.

2 Introduction

The mechano-electrical transduction (MET) complex of sensory hair cells is an assembly of proteins and lipids that facilitate the conversion of auditory, vestibular and hydrodynamic stimuli into electrical signals. Our current understanding is that the proteins of the MET complex consist of the tip link proteins cadherin 23 (CDH23) and protocadherin 15 (PCDH15) at the upper and lower ends of the tip link respectively (Kazmierczak et al., 2007), the pore-forming subunits transmembrane channel-like proteins TMC1 and TMC2 (Kawashima et al., 2011; Pan et al., 2013, 2018), and the accessory subunits transmembrane inner ear (TMIE) and lipoma HMGIC fusion partner-like 5 (LHFPL5) (Cunningham and Müller, 2019; Xiong et al., 2012; Zhao et al., 2014). How these proteins are correctly localized to the sensory hair bundle and assemble into a functional complex is a fundamental question for understanding the molecular basis of how mechanotransduction occurs.

Recent studies have revealed extensive biochemical interactions between the MET complex proteins that are required for the function and / or stable integration of each component in the complex. In particular, LHFPL5 is a central player in MET complex formation, stability, and function. LHFPL5 (a.k.a. tetraspan membrane protein of the hair cell stereocilia / TMHS) is a four transmembrane domain protein from the superfamily of tetraspan junctional complex proteins. This superfamily includes junctional proteins like claudins and connexins, as well as ion channel auxiliary subunits such as transmembrane α-amino-3-hydroxy-5-methyl-4-isoxazole propionic acid receptor (AMPAR) regulatory proteins (TARPs) and the gamma subunits of voltage gated calcium channels. Pathogenic mutations in LHFPL5 are a cause of non-syndromic sensorineural hearing loss in humans (DFNB67), mice and zebrafish (Longo-Guess et al., 2005; Nicolson et al., 1998; Obholzer et al., 2012; Shabbir et al., 2006). LHFPL5 localizes to the tips of stereocilia (Li et al., 2019; Mahendrasingam et al., 2017; Xiong et al., 2012) where it directly interacts with other MET complex components. Co-immunoprecipitation experiments in heterologous cells suggests that LHFPL5 can directly interact with PCDH15 and TMIE (Xiong et al., 2012; Zhao et al., 2014). A structure of the PCDH15 - LHFPL5 complex has also been reported (Ge et al., 2018).

A precise role for LHFPL5 has yet to be defined. One current hypothesis is that LHFPL5 acts as an auxiliary subunit of the MET channel to stabilize the complex, similar to TARPs and the gamma subunits of voltage-gated calcium channels. In mouse cochlear hair cells, PCDH15 and LHFPL5 require each other for stable localization at the tips of stereocilia (Mahendrasingam et al., 2017; Xiong et al., 2012), consistent with their well-defined biochemical interaction. The partial loss of PCDH15 from the stereocilia explains the observed reduction in the number of tip links and the dysmorphic hair bundles in *Lhfpl5*$^{-/-}$ hair cells. Interestingly, although experiments have failed to demonstrate a biochemical interaction between LHFPL5 and the TMCs, LHFPL5 is required for the localization of TMC1, but not TMC2, in the hair bundle of mouse cochlear hair cells (Beurg et al., 2015). Consistent with this finding, the researchers identified a residual TMC2-dependent MET current in *Lhfpl5* mutant mice. The basis for the selective loss of TMC1 is not known.

In zebrafish, Lhfpl5a plays a similar role in mechanotransduction as its mammalian counterparts. A mutation in zebrafish *lhfpl5a* was reported in a forward genetic screen for genes required for hearing and balance (Nicolson et al., 1998; Obholzer et al., 2012). The loss of Lhfpl5a disrupts the targeting of Pcdh15a to stereocilia and results in splayed hair bundles (Maeda et al., 2017). However, Lhfpl5a is not required to correctly localize Tmie and vice versa (Pacentine and Nicolson, 2019), in spite of their biochemical interaction in cultured cells (Xiong et al., 2012). Lhfpl5 still localizes to the tips of stereocilia in *Tmc1*/*Tmc2* double mutants (Beurg et al., 2015), as well as *transmembrane O-methyltransferase* (*tomt*) mouse and zebrafish mutants, which fail to traffic TMCs to the hair bundle

This is a provisional file, not the final typeset article

(Cunningham et al., 2017; Erickson et al., 2017). This phenotype suggests that Lhfpl5 localization does not require the TMCs. However, a number of questions regarding the functions of Lhfpl5 remain unanswered: 1) In zebrafish, what are the molecular requirements for targeting Lhfpl5a to the hair bundle? 2) Is the Lhfpl5-dependent targeting of Tmc1 to the hair bundle an evolutionarily-conserved aspect of their interaction? 3) *lhfpl5a* mutants have defects in auditory and vestibular behaviors, yet sensory hair cells of the lateral line are unaffected (Nicolson et al., 1998). What is the genetic basis for the persistence of lateral line function in *lhfpl5a* mutants?

In this work, we report that teleost fish have two *lhfpl5* genes, *lhfpl5a* and *lhfpl5b*. The zebrafish *lhfpl5* ohnologs are expressed in distinct populations of larval sensory hair cells: *lhfpl5a* in the auditory and vestibular system; *lhfpl5b* in the hair cells of the lateral line organ. Their divergent expression patterns explain why lateral line hair cells are still mechanically-sensitive in *lhfpl5a* mutants. CRISPR-Cas 9 knockout of *lhfpl5b* alone silences the lateral line organ but has no effect on otic hair cell function. We also show that neither Lhfpl5a nor Lhfpl5b are required for Tmc localization in stereocilia. Additionally, we use a GFP-tagged Lhfpl5a to demonstrate that Myo7aa and the tip link proteins Cdh23 and Pcdh15a are required for proper Lhfpl5a localization in otic hair cell bundles. This study reveals the subfunctionalization of the zebrafish *lhfpl5* ohnologs through the divergence in their expression patterns. Furthermore, our work complements previous results from murine cochlear hair cells by highlighting a conserved association between Lhfpl5 and Pcdh15, but also demonstrating novel requirements for Cdh23 and Myo7aa in localizing Lhfpl5a. Lastly, our work indicates that Lhfpl5-dependent localization of Tmc1 is not a universal feature of sensory hair cells and that Lhfpl5 proteins are required for mechanotransduction independently of a role in localizing the Tmc channel subunits to stereocilia.

3 Materials and Methods

3.1 Ethics statement

Animal research complied with guidelines stipulated by the Institutional Animal Care and Use Committees at Oregon Health and Science University (Portland, OR, USA) and East Carolina University (Greenville, NC, USA). Zebrafish (*Danio rerio*) were maintained and bred using standard procedures (Westerfield, 2000).

3.2 Mutant and transgenic fish lines

The following zebrafish mutant alleles were used for this study: *cdh23*^{nl9}, *cdh23*^{tj264}, *lhfpl5a*^{tm290d}, *lhfpl5b*^{vo35}, *myo7aa*^{ty220}, *pcdh15a*^{psi7}, *pcdh15a*^{th263b} (Erickson et al., 2017; Ernest et al., 2000; Maeda et al., 2017; Nicolson et al., 1998; Obholzer et al., 2012). The transgenic lines used in this study were *Tg(-6myo6b:eGFP-lhfpl5a)vo23Tg*, *Tg(-6myo6b:tmc1-emGFP)vo27Tg*, *Tg(-6myo6b:tmc2b-emGFP)vo28Tg* (Erickson et al., 2017), and *Tg(-6myo6b:eGFP-pA)vo68Tg*. All experiments used larvae at 1–7 dpf, which are of indeterminate sex at this stage.

3.3 Genotyping

Standard genomic PCR followed by Sanger sequencing was used to identify *cdh23*^{tj264}, *cdh23*^{nl9}, *lhfpl5a*^{tm290d}, *pcdh15a*^{psi7}, and *pcdh15a*^{th263b} alleles. The *lhfpl5b*^{vo35} mutation disrupts a MluCI restriction site (AATT) and we are able to identify *lhfpl5b*^{vo35} hetero- and homozygotes based on the different sizes of MluCI-digested PCR products resolved on a 1.5% agarose gel. The following primers were used for genotyping:

124 *cdh23*^{nl9}: Fwd – CCACAGGAATTCTGGTGTCC, Rvs – GAAAGTGGGCGTCTCATCAT;

125 *cdh23*^{tj264}: Fwd – GGACGTCAGTGTTCATGGTG, Rvs – TTTTCTGACCGTGGCATTAAC;

126 *lhfpl5a*^{tm290d}: Fwd – GGACCATCATCTCCAGCAAAC, Rvs –
127 CACGAAACATATTTTCACTCACCAG;

128 *lhfpl5b*^{vo35}: Fwd – GCGTCATGTGGGCAGTTTTC, Rvs – TAGACACTAGCGGCGTTGC;

129 *myo7aa*^{ty220}: Fwd – TAGGTCCTCTTTAATGCATA, Rvs –
130 GTCTGTCTGTCTGTCTATCTGTCTCGCT;

131 *pcdh15a*^{psi7}: Fwd – TTGGCACCACTATCTTTACCG, Rvs – ACAGAAGGCACCTGGAAAAC;

132 *pcdh15a*^{th263b}: Fwd – AGGGACTAAGCCGAAGGAAG, Rvs –
133 CACTCATCTTCACAGCCATACAG.

134 **3.4 Phylogeny**

135 Lhfpl5 protein sequences retrieved from either NCBI or Ensembl (Supplemental Table 1).
136 Phylogenetic analysis was done on www.phylogeny.fr using T-Coffee (multiple sequence alignment),
137 GBlocks (alignment curation), PhyML (maximum likelihood tree construction with 100 replicates to
138 estimate bootstrap values), and TreeDyn (visualization) (Dereeper et al., 2008).

139 **3.5 mRNA *in situ* hybridization**

140 *lhfpl5a* and *lhfpl5b* probe templates were amplified from total RNA using the following primers:
141 *lhfpl5a* Fwd: AATATTGGTGCATAGACTCAAGGAGG; Rvs:
142 GACTCCAAAATGACCTTTTAACAAACGC. *lhfpl5b* Fwd:
143 TGAAGATCAGCTACGATATAACCGG; Rvs: ACTGTGATTGGTGTATTTCCAGC. The inserts
144 were cloned into the pCR4 vector for use in probe synthesis. mRNA *in situ* probe synthesis and
145 hybridization was performed essentially as previously described (Erickson et al., 2010; Thisse and
146 Thisse, 2008). Stained specimens were mounted on a depression slide in 1.2 % low-melting point
147 agarose and imaged on a Leica DMLB microscope fitted with a Zeiss AxioCam MRc 5 camera using
148 Zeiss AxioVision acquisition software (Version 4.5).

149 **3.6 Immunofluorescent staining, FM dye labeling, and fluorescence microscopy**

150 Anti-Pcdh15a immunostaining and FM dye labeling of inner ear and lateral line hair cells were
151 performed as previously described (Erickson et al., 2017). All fluorescent imaging was done on Zeiss
152 LSM 700 or LSM 800 laser scanning confocal microscopes. Z-stacks were analyzed using ImageJ
153 (Schneider et al., 2012). All related control and experimental images were adjusted equally for
154 brightness and contrast in Adobe Photoshop CC.

155 **3.7 CRISPR-Cas9 knockout of *lhfpl5b***

156 An sgRNA targeting the *lhfpl5b* sequence 5'- CAACCCAATCACCTCGGAAT-3' was synthesized
157 essentially as described (Gagnon et al., 2014). For microinjection, 1 µg of sgRNA was mixed with 1
158 ug of Cas9 protein and warmed to 37ºC for 5 minutes to promote the formation of the Cas9-sgRNA
159 complex. Approximately 2 nl of this solution was injected into wild type embryos at the single-cell
160 stage. Efficacy of cutting was determined in two ways: 1) Single larvae genotyping - Amplification of

This is a provisional file, not the final typeset article

161 the target genomic region by PCR and running the products on 2.5% agarose gels to assay for disruption
162 of a homogenous amplicon. 2) Assaying for disruption of the mechanotransduction channel in lateral
163 line hair cells by FM 1-43 dye uptake. Larvae displaying a non-wild type pattern of FM 1-43 dye uptake
164 were raised to adulthood. Progeny from in-crosses of F0 adults were exposed to FM 1-43 dye to identify
165 founders. By outcrossing founder adults, we established a line of fish carrying a 5 base pair deletion in
166 the *lhfpl5b* coding region that causes a S77FfsX48 mutation (*lhfpl5b*^{vo35}). This mutation disrupts the
167 protein in the first extracellular loop and deletes the final three of four transmembrane helices in
168 Lhfpl5b.

169 **3.8 Acoustic startle response**

170 Quantification of the larval acoustic startle response was performed using the Zebrabox monitoring
171 system (ViewPoint Life Sciences, Montreal, Canada) as previously described (Maeda et al., 2017) with
172 the following modifications. Each trial included six larvae which were subjected to two or three trials
173 of 6 acoustic stimuli. For each individual larva, the trial with best AEBR performance was used for
174 quantification. Positive responses where spontaneous movement occurred in the second prior to the
175 stimulus were excluded from analysis. Trials where spontaneous movement occurred for more than 6
176 of the 12 stimuli were also excluded from analysis.

177 **3.9 Microphonics**

178 We performed the microphonic measurements as previously described (Pacentine and Nicolson, 2019).
179 In brief, we anesthetized 3 dpf larvae in extracellular solution (140 mM NaCl, 2 mM KCl, 2 mM $CaCl_2$,
180 1 mM $MgCl_2$, and 10 mM 4-(2-hydroxyethyl)-1-piperazineethanesulfonic acid (HEPES); pH 7.4)
181 containing 0.02% 3-amino benzoic acid ethylester (MESAB; Western Chemical). We pinned the larvae
182 with two glass fibers straddling the yolk and a third perpendicular fiber to prevent sliding. For pipettes,
183 we used borosilicate glass with filament, O.D.: 1.5 mm, O.D.: 0.86 mm, 10 cm length (Sutter, item #
184 BF150-86-10, fire polished). Using a Sutter Puller (model P-97), we created recording pipettes with a
185 long shank with a resistance of 10-20 MΩ, after which we beveled the edges to a resistance of 4-5 MΩ
186 using a Sutter Beveler with impedance meter (model BV-10C). For the glass probe delivering the piezo
187 stimulus, we pulled a long shank pipette and fire polished to a closed bulb. We shielded the apparatus
188 with tin foil to completely ground the piezo actuator. To maintain consistent delivery of stimulus, we
189 always pressed the probe to the front of the head behind the lower eye, level with the otoliths in the ear
190 of interest. We also maintained a consistent entry point dorsal to the anterior crista and lateral to the
191 posterior crista. During delivery of stimulus, the piezo probe made light contact with the head. We
192 drove the piezo with a High Power Amplifier (piezosystem jena, System ENT/ENV, serial # E18605),
193 and recorded responses in current clamp mode with a patch-clamp amplifier (HEKA, EPC 10 usb
194 double, serial # 550089). Voltage responses were amplified 1000x and filtered between 0.1 - 3000 Hz
195 by the Brownlee Precision Instrumentation Amplifier (Model 440). We used a 200 Hz sine wave
196 stimulus at 10 V and recorded at 20 kHz, collecting 200 traces per experiment. Each stimulus was of
197 40 ms duration, with 20 ms pre- and post-stimulus periods. The piezo signal was low-pass filtered at
198 500 Hz using the Low-Pass Bessel Filter 8 Pole (Warner Instruments). In Igor Pro, we averaged each
199 set of 200 traces to generate one wave response per larva. To quantify hair cell activity, we calculated
200 the amplitude from base-to-peak of the first peak. Larvae were genotyped as described above.

201 **3.10 Hair cell counts**

202 *lhfpl5b*$^{vo35/+}$ fish were crossed with *Tg(myo6b:eGFP-pA)vo68Tg; lhfpl5b*$^{vo35/+}$ fish to produce wild type
203 and *lhfpl5b*^{vo35} siblings expressing green fluorescent protein in hair cells. Wild type and *lhfpl5b* mutant
204 larvae were sorted by FM 4-64 labeling (n = 11 each). In experiment 1, larvae (n = 5 each genotype)

were fixed in 4% paraformaldehyde at 5 dpf. In experiment 2, larvae (n = 6 each genotype) were imaged immediately. *lhfpl5a*$^{tm290d/+}$ fish were in-crossed to produce wild type and *lhfpl5a*^{tm290d} siblings. Larvae were sorted based on the auditory and vestibular defects associated with the *lhfpl5a*^{tm290d} homozygous mutants. Larvae were labelled with FM 1-43 (n = 6 each). For all experiments, specimens were mounted in low melting point agarose and the L1, MI1, and O2 neuromasts were imaged on a Zeiss LSM 800 confocal. Cell counts were performed using the Z-stack data.

3.11 Statistics

Statistical analyses were done using the R stats package in RStudio (R Core Team, 2019; RStudio Team, 2018). P-values of less than 0.05 were considered to be statistically significant. Plots were made with ggplot2 (Wickham, 2016).

3.12 Data availability

The raw data supporting the conclusions of this manuscript will be made available by the corresponding author, without undue reservation, to any qualified researcher.

4 Results

4.1 Teleost fish have ohnologous *lhfpl5* genes.

Genes that have been duplicated as a result of a whole genome duplication (WGD) event are known as *ohnologs* (Ohno, 1970; Wolfe, 2000). Due to the teleost-specific WGD, it is not uncommon to find ohnologous genes in teleost fish where other vertebrate classes possess a single gene. The *Danio rerio* (zebrafish) genome contains two *lhfpl5* genes: *lhfpl5a* (ENSDARG00000045023) and *lhfpl5b* (ENSDARG00000056458). To determine if *lhfpl5* duplication is general to the teleost lineage, we queried either GenBank or Ensembl databases to collect Lhfpl5 protein sequences for humans, mice, chick, frogs, and representative sequences from 14 phylogenetic orders of ray-finned fish (Actinopterygii), including 13 orders from the Teleostei infraclass and one from the Holostei infraclass (Supplemental Table 1). The latter (Spotted gar, *Lepisosteus oculatus*) is commonly used to infer the consequences of the teleost WGD, since the Holostei and Teleostei infraclasses diverged before the teleost WGD (Braasch et al., 2016). Phylogenetic analysis of the Lhfpl5 protein sequences supports the idea that duplicate *lhfpl5* genes originated from the teleost WGD event (Figure 1A). In all 13 teleost orders surveyed, there are two *lhfpl5* genes whose protein products cluster with either the *lhfpl5a* or *lhfpl5b* ohnolog groups. Based on available genomic data, there is no evidence that spotted gar fish have duplicated *lhfpl5* genes. Nor is there evidence that the Salmonid-specific WGD (Allendorf and Thorgaard, 1984) lead to further expansion of the *lhfpl5* family. These analyses suggest that the ancestral *lhfpl5* gene was duplicated in the teleost WGD and that the *lhfpl5* ohnologs were retained in all teleost species examined here.

Alignment of the zebrafish Lhfpl5a and Lhfpl5b proteins with those from human, mouse and chicken reveals that both zebrafish ohnologs retain the same protein structure (Figure 1B). Zebrafish Lhfpl5a and Lhfpl5b are 76% identical and 86% similar to one another (Needleman-Wunsch alignment). Compared to human LHFPL5, Lhfpl5a and Lhfpl5b are 70 / 65 % identical and 86 / 81 % similar respectively. The ENU-generated mutation in *lhfpl5a* (*tm290d*) (Obholzer et al., 2012) is indicated by the red triangle (K80X). To investigate the function of *lhfpl5b*, we generated a Cas9-induced lesion in the *lhfpl5b* gene in a similar location as the *tm290d* mutation. We recovered a line with a 5 base pair deletion leading to a frameshift mutation (*lhfpl5b*^{vo35}, red square; S77FfsX48).

This is a provisional file, not the final typeset article

248 **4.2 *lhfpl5a* and *lhfpl5b* are expressed in distinct populations of sensory hair cells.**

249 To characterize the spatial and temporal patterns of *lhfpl5a/b* gene expression, we performed whole
250 mount mRNA *in situ* hybridization on zebrafish larvae at 1, 2, and 5-days post-fertilization (dpf)
251 (Figure 2). After one day of development, there are nascent hair cells of the presumptive anterior and
252 posterior maculae in the developing ear, but no lateral line hair cells at this stage. We detect *lhfpl5a*
253 expression in the presumptive anterior and posterior maculae at 1 dpf (Figure 2A). No signal for *lhfpl5b*
254 was observed at this time point (Figure 2B). At 2 dpf, we observe a clear distinction in the expression
255 patterns of the *lhfpl5a* and *lhfpl5b* genes (Figure 2C, D). *lhfpl5a* continues to be expressed in the ear,
256 but expression is not observed in the newly deposited neuromasts. Conversely, we detect *lhfpl5b*
257 expression exclusively in neuromasts at this stage, both on the head (Figure 2D) and trunk (data not
258 shown). This divergence in *lhfpl5* ohnolog expression continues at 5 dpf, with *lhfpl5a* found
259 exclusively in the sensory patches of the ear and *lhfpl5b* restricted to lateral line hair cells (Figure 2E-
260 J). Taken together, our results suggest that both *lhfpl5a* and *lhfpl5b* have been retained since the teleost
261 whole genome duplication because of their non-overlapping mRNA expression patterns.

262 **4.3 *lhfpl5a* mediates mechanosensitivity of otic hair cells.**

263 *lhfpl5a*^{tm290d} (*astronaut / asn*) mutants were initially characterized by balance defects, an absence of
264 the acoustic startle reflex, and a lack of brainstem Ca^{2+} signals after acoustic startle. However,
265 neuromast microphonic potentials were normal (Nicolson et al., 1998). In light of our *in situ*
266 hybridization data (Figure 2), these results suggest that *lhfpl5a* is required for auditory and vestibular
267 hair cell function only. To test this possibility, we performed several functional assays measuring the
268 activity of hair cells in the otic capsule. First, we tested macular hair cell activity (Lu and DeSmidt,
269 2013; Yao et al., 2016) by recording extracellular microphonic potentials from the inner ears of
270 *lhfpl5a*^{tm290d} mutants, along with wild type and *lhfpl5b*^{vo35} larvae at 3 dpf. We then measured baseline-
271 to-peak amplitude of the first peak to quantify activity (Supplemental Figure 1A-D). Consistent with
272 the initial characterization of the behavioral defects in *lhfpl5a*^{tm290d} mutants, we did not detect robust
273 microphonic potentials from the inner ear of *lhfpl5a*^{tm290d} mutants (Figure 3A). We measured an
274 average first peak microphonic of 53.1 μV from *lhfpl5a*^{tm290d} mutants ($n = 7$), which was significantly
275 less than the 296.2 μV average value of their WT siblings ($n = 5$; $p = 0.01$, Welch's t-test). We believe
276 that at least some of the signal detected in *lhfpl5a*^{tm290d} mutants may be a stimulus artefact due the
277 unusual rise time and similar observations we have made in other known transduction-null mutants.

278 For the *lhfpl5b*^{vo35} mutants ($n = 6$), we measured an average first peak microphonic potential of 280.9
279 μV. These values were not significantly different from their WT siblings ($n = 4$, average 243.8 μV; p
280 = 0.7) but were significantly greater than the *lhfpl5a*^{tm290d} mutants ($p = 0.036$). Thus, *lhfpl5a*^{tm290d}
281 mutants exhibit defects in inner ear function, while the *lhfpl5b*^{vo35} mutation has no effect on these hair
282 cells. To further confirm the lack of inner ear function in *lhfpl5a*^{tm290d} mutants, we performed an
283 acoustic startle test on larvae at 6 dpf (Figure 3B). Results confirm that *lhfpl5a*^{tm290d} mutants are
284 profoundly deaf, displaying little to no response to acoustic stimuli ($p < 0.001$ compared to all other
285 genotypes). Finally, we examined the basal MET channel activity of hair cells of the inner ear by
286 injecting FM 4-64 into the otic capsule and imaging the lateral cristae sensory patch. WT hair cells
287 readily labeled with FM 4-64 whereas *lhfpl5a*^{tm290d} mutant cells showed no sign of dye internalization
288 (Figure 3C-D). These three tests confirmed that all sensory patches in the otic capsule are inactive in
289 *lhfpl5a*^{tm290d} mutants.

290 A *GFP-lhfpl5a* transgenic line of zebrafish - *Tg(myo6b:eGFP-lhfpl5a)vo23Tg* - has been reported
291 previously (Erickson et al., 2017). GFP-Lhfpl5a is present at the tips of stereocilia, similar to the
292 localization observed for mouse LHFPL5 (Mahendrasingam et al., 2017; Xiong et al., 2012). To

293 demonstrate that the GFP-Lhfpl5a protein is functional, we assayed for rescue of the acoustic startle
294 reflex and MET channel activity in homozygous *lhfpl5a*^{tm290d} mutants expressing the transgene. The
295 startle reflex of *lhfpl5a*^{tm290d} mutants expressing GFP-Lhfpl5a were statistically indistinguishable from
296 non-transgenic and transgenic WT siblings (p = 0.48 and 0.26 respectively; Figure 3B). Likewise, FM
297 4-64 dye-labeling in the inner ear was restored to *lhfpl5a*^{tm290d} mutants expressing GFP-Lhfpl5a (Figure
298 3E-F'). From these results we conclude that the hair bundle-localized GFP-Lhfpl5a protein is
299 functional and can rescue the behavioral and MET channel defects in *lhfpl5a*^{tm290d} mutants.

300 **4.4 *lhfpl5b* mediates mechanosensitivity of lateral line hair cells.**

301 The divergent expression patterns of the *lhfpl5* ohnologs suggests that *lhfpl5b* alone may be mediating
302 mechanosensitivity of lateral line hair cells. To test this, we compared basal MET channel activity in
303 neuromast hair cells of WT, *lhfpl5a*^{tm290d} and *lhfpl5b*^{vo35} larvae using an FM 1-43 dye uptake assay
304 (Figure 4A-C). Strikingly, lateral line hair cells in *lhfpl5b*^{vo35} mutants do not label with FM 1-43 while
305 there is no difference in the intensity of FM 1-43 labeling of hair cells between WT and *lhfpl5a*^{tm290d}
306 mutants (Figure 4A-C, Supplemental Figure 2A - C). We quantified this loss of lateral line function in
307 *lhfpl5b* mutants by measuring the average FM 1-43 fluorescence intensity per hair cell in each imaged
308 neuromast of *lhfpl5b*^{vo35} mutants and wild type siblings at 2 dpf (Figure 4D, E, H) and 5 dpf (Figure
309 4F-H). *lhfpl5b*^{vo35} mutants exhibit a statistically significant decrease in FM 1-43 uptake at both 2 dpf
310 and 5 dpf (Welch's *t*-test, $p < 0.001$ both time points). While there is negligible FM dye labeling in the
311 vast majority of *lhfpl5b*^{vo35} mutant neuromasts, we occasionally observe labeling in some hair cells,
312 most reproducibly in the SO3 neuromast. Occasional labeling persists in *lhfpl5a* / *lhfpl5b* double
313 mutants, indicating that *lhfpl5a* is not partially compensating for the loss of *lhfpl5b* (Supplemental
314 Figure 3A-D). The loss of MET channel activity in *lhfpl5b*^{vo35} neuromasts is rescued by expression of
315 the *GFP-lhfpl5a vo23Tg* transgene (Figure 4I, J; n = 7/7 mutant individuals). This result indicates that
316 Lhfpl5a and Lhfpl5b are functionally interchangeable in this context.

317 We have previously reported a reduced number of neuromast hair cells in other transduction mutants
318 such as *myo7aa (mariner)*, *pcdh15a (orbiter)*, and *tomt (mercury)* (Erickson et al., 2017; Seiler et al.,
319 2005). The ultimate cause for this reduction in hair cell number is not known. If *lhfpl5b*^{vo35} mutants are
320 defective in mechanotransduction, we would expect a similar decrease in the number of neuromast hair
321 cells. To test this idea, we compared hair cell counts between wild type, *lhfpl5a*^{tm290d}, and *lhfpl5b*^{vo35}
322 larvae at 5 dpf. As expected, wild type and *lhfpl5a*^{tm290d} mutants have statistically equivalent numbers
323 of hair cells in the neuromasts surveyed (Supplemental Figure 2D, p = 0.58). In *lhfpl5b*^{vo35} mutant
324 neuromasts, we observe a statistically significant decrease in the number of hair cells (Figure 4K,
325 n = 11 individuals per genotype, 3 NM each, $p < 0.001$ each NM type by Welch's *t*-test; representative
326 neuromasts are shown in Supplemental Figure 4). This decrease in the number of neuromast hair cells
327 is consistent with *lhfpl5b* mutants being deficient in mechanotransduction in this cell type.

328 **4.5 *lhfpl5* is not required for Tmc localization to the hair bundle in zebrafish hair cells.**

329 Previous studies have demonstrated that loss of LHFPL5 leads to a ~90% reduction in the peak
330 amplitude of the transduction current in mouse cochlear outer hair cells (Xiong et al., 2012). Single
331 channel recordings from *Lhfpl5* mutants revealed that the remaining transduction current in *Lhfpl5*
332 mutants was mediated by TMC2 (Beurg et al., 2015). Using antibodies to detect endogenous protein,
333 TMC1 was found to be absent from the bundle of *Lhfpl5* mouse mutants. However, injectoporated
334 Myc-TMC2 was still able to localize to the hair bundle, supporting the idea that LHFPL5 is required
335 for the targeting of TMC1, but not TMC2. The localization of exogenously-expressed TMC1 in *Lhfpl5*
336 mutants was not reported.

This is a provisional file, not the final typeset article

337 To determine if the Tmcs require Lhfpl5a for localization to the hair bundle of zebrafish hair cells, we
338 bred stable transgenic lines expressing GFP-tagged versions of Tmc1 (*vo27Tg*) and Tmc2b (*vo28Tg*)
339 (Erickson et al., 2017) into the *lhfpl5a*^{tm290d} mutant background and imaged Tmc localization in the
340 lateral cristae of the ear. In contrast to what was observed in mouse cochlear hair cells, both Tmc1-
341 GFP and Tmc2b-GFP are still targeted to the hair bundle in *lhfpl5a*^{tm290d} mutants (n = 11/11 and 9/9
342 individuals respectively; Figure 5A-D'). We also observe Tmc2b-GFP localization in the neuromast
343 hair bundles of *lhfpl5b*^{vo35} mutants (n = 7/7 individuals; Figure 5E-F'). Additionally, we do not observe
344 any rescue of hair cell function in *lhfpl5b* mutants expressing the Tmc2b-GFP protein (Supplemental
345 Figure 5A-C). As such, these results suggest that GFP-tagged Tmc1 and Tmc2b do not require Lhfpl5
346 for hair bundle localization in zebrafish hair cells.

347 **4.6 GFP-Lhfpl5a localization in stereocilia requires Pcdh15a, Cdh23, and Myo7aa.**

348 Previous work has shown that PCDH15 and LHFPL5 are mutually dependent on one another to
349 correctly localize to the site of mechanotransduction in mouse cochlear hair cells (Mahendrasingam et
350 al., 2017; Xiong et al., 2012). Likewise in zebrafish, Lhfpl5a is required for proper Pcdh15a
351 localization in the hair bundle, as determined Pcdh15a immunostaining and the expression of a
352 Pcdh15a-GFP transgene in *lhfpl5a*^{tm290d} mutants (Maeda et al., 2017). Using the previously
353 characterized antibody against Pcdh15a, we observe the highest level of Pcdh15a staining at the apical
354 part of the hair bundle, with less intense punctate staining throughout the stereocilia in 3 dpf wild type
355 larvae (Figure 6A). *lhfpl5a*^{tm290d} mutants exhibit splayed hair bundles, with low levels of Pcdh15a
356 staining restricted to the tip of each stereocilium (n = 5/5 individuals; Figure 6B), confirming our
357 previous report.

358 To determine if Lhfpl5a also depends on Pcdh15a for its localization, we imaged GFP-Lhfpl5 in the
359 lateral cristae of *pcdh15a*^{psi7} homozygous mutants. In wild type larvae, GFP-Lhfpl5a is distributed
360 throughout the hair bundle at the tips of stereocilia (yellow arrow heads), with a higher intensity of
361 GFP evident in the tallest rows, possibly at the sites of kinociliary links (Figure 6C, C', arrow). In
362 *pcdh15a*^{psi7} mutants, GFP-Lhfpl5a is absent from the hair bundle except for the tallest rows of
363 stereocilia adjacent to the kinocilium (n = 4 individuals; Figure 6D, D', arrow). We observed similar
364 results using the *pcdh15a*^{th263b} allele (n = 6/6 individuals; Supplemental Figure 6A, B). Consistent with
365 our earlier studies (Maeda et al., 2017; Seiler et al., 2005), we observe splayed hair bundles in both
366 *pcdh15a* alleles suggesting a loss of connections and tip links between the stereocilia. These results
367 indicate that GFP-Lhfpl5a requires Pcdh15a for stable targeting to the shorter stereocilia, but Pcdh15a
368 is not required for retaining GFP-Lhfpl5a in the tallest rows of stereocilia adjacent to the kinocilium.

369 The observation that some GFP-Lhfpl5a signal remains in the tallest stereocilia of *pcdh15a* mutants
370 suggests that additional proteins are involved in targeting Lhfpl5a to these sites in zebrafish vestibular
371 hair cells. Previous research has shown that mouse CDH23 still localizes to tips of stereocilia in
372 PCDH15-deficient mice (Boëda et al., 2002; Senften et al., 2006) and that CDH23 is a component of
373 kinociliary links (Goodyear et al., 2010; Siemens et al., 2004). Based on these reports, we tested
374 whether Cdh23 was required for GFP-Lhfpl5a localization. In *cdh23*^{nl9} mutants, GFP-Lhfpl5 is
375 sparsely distributed throughout the length of the kinocilium (n = 4/4 individuals, Figure 6E, E'). We
376 also observe a redistribution of GFP-Lhfpl5a into the kinocilium using the *cdh23*^{tj264} allele (n = 4/4
377 individuals; Supplemental Figure 6C). In both *cdh23* alleles, we see occasional GFP signal in the
378 stereocilia as well, though this localization is not as robust. Interestingly, these results contrast with
379 those from mouse cochlear hair cells which showed that Lhfpl5 does not require Cdh23 for bundle
380 localization (Zhao et al., 2014). The same study also could not detect any biochemical interaction
381 between LHFPL5 and proteins of the upper tip link density including CDH23, USH1C / Harmonin, or

USH1G / Sans. Together, our data indicate an unexpected role for Cdh23 in the localization of GFP-Lhfpl5a to the region of kinocilial links in zebrafish vestibular hair cells.

Myosin 7A (MYO7A) is an actin-based motor protein required for the localization of many proteins of the hair bundle, including PCDH15 and USH1C / Harmonin, along with several proteins of the Usher type 2 complex (Boëda et al., 2002; Lefevre et al., 2008; Maeda et al., 2017; Morgan et al., 2016; Senften et al., 2006; Zou et al., 2017). Results in both mice and zebrafish suggest that MYO7A is not required for CDH23 bundle localization (Blanco-Sanchez et al., 2014; Senften et al., 2006). However, its role in Lhfpl5 localization has not been examined. In *myo7aa*^{ty220} (*mariner*) mutant hair cells, GFP-Lhfpl5a localization in hair bundle is severely disrupted (n = 5/5 individuals; Figure 6 F, F'). We observe GFP signal near the base of hair bundles and occasionally in stereocilia (yellow arrowheads), but do not see robust Lhfpl5a localization in the presumptive kinocilial links nor to the kinocilium itself. Taken together, our results using the GFP-Lhfpl5a transgene suggest that Pcdh15a, Cdh23, and Myo7aa all play distinct roles in Lhfpl5 localization in the bundle of zebrafish vestibular hair cells.

5 Discussion

In this study, we provide support for the following points: 1) The ancestral *lhfpl5* gene was likely duplicated as a result of the teleost whole genome duplication, leading to the *lhfpl5a* and *lhfpl5b* ohnologs described in this paper. 2) In zebrafish, there has been subfunctionalization of these genes as a result of their divergent expression patterns. As determined by mRNA *in situ* hybridization, *lhfpl5a* is expressed only in auditory and vestibular hair cells of the ear while *lhfpl5b* is expressed solely in hair cells of the lateral line organ. Consistent with their expression patterns, we show that each ohnolog mediates mechanotransduction in the corresponding populations of sensory hair cells in zebrafish. 3) Targeting of GFP-tagged Tmcs to the hair bundle is independent of Lhfpl5a function. 4) Proper targeting of GFP-tagged Lhfpl5a to the hair bundle requires the tip link protein Pcdh15a, but as in mice, Lhfpl5a can localize to regions of the hair bundle independently of Pcdh15 function. Additionally, we demonstrate novel requirements for Cdh23 and the Myo7aa motor protein in Lhfpl5 localization.

5.1 Duplicated zebrafish genes in hair cell function.

With regards to genes involved in hair cell function, the zebrafish duplicates of *calcium channel, voltage-dependent, L type, alpha 1D* (*cacna1d* / *cav1.3*), *C-terminal binding protein 2* (*ctbp2* / *ribeye*), *myosin 6* (*myo6*), *otoferlin* (*otof*), *pcdh15*, and *tmc2* have been analyzed genetically. In the cases of *cacna1db*, *pcdh15b* and *myo6a*, these ohnologs are no longer functional in hair cells (Seiler et al., 2004, 2005; Sidi et al., 2004). For the *ctbp2*, *otoferlin*, and *tmc2* duplicates, both genes are required in at least partially overlapping populations of hair cells (Chou et al., 2017; Lv et al., 2016; Maeda et al., 2014; Sheets et al., 2011). In contrast, our results for the *lhfpl5* ohnologs suggest that each gene is expressed and functionally required in distinct, non-overlapping hair cell lineages. To our knowledge, this is the first description of duplicated genes whose expression patterns have cleanly partitioned between inner ear and lateral line hair cells.

5.2 Subfunctionalization of zebrafish *lhfpl5* ohnologs.

We constructed a phylogenetic tree using publicly available Lhfpl5 protein sequence data (Figure 1) Our results suggest that the ancestral *lhfpl5* gene was duplicated during the teleost WGD event and that both genes have been retained throughout the teleost lineage (Figure 1). Our conclusion that *lhfpl5a* and *lhfpl5b* are ohnologs is substantiated by a recent study of ohnologs in teleosts (Singh and Isambert, 2019). In all four teleost species surveyed, Singh and Isambert show that *lhfpl5a* and *lhfpl5b* are true ohnologs that arose from the teleost-specific WGD under the strictest criteria used in their study.

This is a provisional file, not the final typeset article

425 Some kind of selection pressure is required for the retention of both gene ohnologs (Glasauer and
426 Neuhauss, 2014). Our in situ hybridization results show that *lhfpl5a* and *lhfpl5b* are expressed in
427 distinct populations of hair cells and support the idea that the zebrafish *lhfpl5* ohnologs were retained
428 because of their divergent expression patterns (Figure 2). Analysis of hair cell function in the different
429 *lhfpl5* mutants agrees with the gene expression results, showing that *lhfpl5a* is required for transduction
430 in the ear while *lhfpl5b* plays the same role in the lateral line organs. However, rescue of the MET
431 channel defects in *lhfpl5b*^{vo35} mutants by GFP-tagged Lhfpl5a suggests that the functions of these
432 ohnologs are at least partially interchangeable. This result is not surprising given the high degree of
433 similarity between the Lhfpl5a and 5b proteins. As such, the subfunctionalization of the *lhfpl5* ohnologs
434 appears to be caused by the divergence in their expression patterns rather than functional differences
435 in their protein products. It is possible that a similar mechanism is responsible for the retention of both
436 genes in other teleost species as well, though the expression patterns of the *lhfpl5* ohnologs have not
437 been examined in other fish.

438 The non-overlapping expression of the *lhfpl5* ohnologs provides us with a unique genetic tool to study
439 lateral line function. Most mechanotransduction mutants in zebrafish disrupt both inner ear and lateral
440 line hair cell function (Nicolson, 2017). As such, we are unable to assess the role of the lateral line
441 independently of auditory and vestibular defects, which are lethal for larval fish. The *lhfpl5b* mutants
442 are adult viable (data not shown) and represent a possible genetic model for understanding the lateral
443 line in both larval and adult fish. Future studies on adults will determine whether the lateral line remains
444 non-functional and whether *lhfpl5b* contributes to inner ear function in the mature auditory and
445 vestibular systems.

446 5.3 The molecular requirements for bundle localization of MET complex proteins differs 447 between mouse and zebrafish hair cells.

448 Our understanding of mechanotransduction at the molecular level is heavily informed by work done
449 using mouse cochlear hair cells. However, analysis of zebrafish inner ear and lateral line hair cells can
450 lead to a more complete picture of how vertebrate sensory hair cells form the MET complex. At their
451 core, the genetic and molecular bases for mechanotransduction are well conserved between mouse and
452 zebrafish hair cells. For example, the tip link proteins Cdh23 and Pcdh15a, MET channel subunits
453 Tmc1/2, Tmie, and Lhfpl5, along with additional factors such as Tomt, Cib2, and Myo7aa are all
454 necessary for MET channel function in both mice and fish (Cunningham et al., 2017; Erickson et al.,
455 2017; Giese et al., 2017; Gleason et al., 2009; Kawashima et al., 2011; Nicolson et al., 1998; Pacentine
456 and Nicolson, 2019; Senften et al., 2006; Siemens et al., 2004; Söllner et al., 2004; Xiong et al., 2012;
457 Zhao et al., 2014). However, while each of these factors are required for mechanotransduction in
458 vertebrate hair cells, the details of how they contribute to MET channel function may differ depending
459 on the particular type of hair cell or the vertebrate species. For example, Tmie is required for Tmc
460 localization to the hair bundle in zebrafish (Pacentine and Nicolson, 2019), but this does not appear to
461 be the case in mouse cochlear hair cells (Zhao et al., 2014). The evolutionary pressures that lead to
462 these differences between mouse and zebrafish hair cells are not understood.

463 Based on multiple lines of evidence gathered from mice, TMC1 and TMC2 have different requirements
464 for LHFPL5 regarding localization to the hair bundle (Beurg et al., 2015). Endogenous TMC1 is absent
465 from the bundle in LHFPL5-deficient cochlear hair cells with the remaining MET current mediated
466 through TMC2. Exogenously-expressed TMC2 is still targeted correctly in *Lhfpl5* mutants, but it was
467 not reported whether the same is true for exogenous TMC1, nor whether similar requirements hold for
468 vestibular hair cells. As such, the role of LHFPL5 in mechanotransduction is not clear: is LHFPL5

469 required primarily for targeting TMC1 to the hair bundle, or does LHFPL5 mediate MET channel
470 function in other ways?

471 For our study, we used stable transgenic lines expressing GFP-tagged Tmc1 and Tmc2b to show that
472 the Tmcs do not require Lhfpl5a for targeting to the stereocilia of zebrafish vestibular hair cells. Nor
473 is Lhfpl5b required for Tmc2b-GFP localization in the hair bundle of neuromast hair cells. The
474 occasional FM labeled-hair cell in *lhfpl5b* and *lhfpl5a/5b* mutant neuromasts is consistent with the
475 continued ability of the Tmcs to localize to the hair bundle. This observation is reminiscent of the
476 sporadic, low level of FM dye labeling in the cochlear hair cells of *Lhfpl5* mutant mice (György et al.,
477 2017). Partial compensation by yet another member of the *lhfpl* family remains as a possible
478 explanation for the remaining basal channel function. Lastly, we find that exogenous Tmc expression
479 does not rescue MET channel activity in either *lhfpl5* mutant zebrafish. Taken together, our results
480 support a Tmc-independent role for Lhfpl5 proteins in mechanotransduction.

481 What then is the role of LHFPL5 in vertebrate mechanotransduction? LHFPL5 and PCDH15 are known
482 to form a protein complex and regulate each other's localization to the site of mechanotransduction in
483 mouse cochlear hair cells (Ge et al., 2018; Mahendrasingam et al., 2017; Xiong et al., 2012). However,
484 their localization to the hair bundle is not completely dependent on one another. For example, tips links
485 are not completely lost in *Lhfpl5*$^{-/-}$ cochlear hair cells and exogenous overexpression of PCDH15
486 partially rescues the transduction defects in *Lhfpl5* mutant mice (Xiong et al., 2012). Similarly, a
487 detailed immunogold study in wild type and *Pcdh15*$^{-/-}$ cochlear hair cells showed that there are
488 PCDH15-dependent and PCDH15-independent sites of LHFPL5 localization (Mahendrasingam et al.,
489 2017). PCDH15 is required for stable LHFPL5 localization at the tips of ranked stereocilia in
490 association with the MET channel complex. However, LHFPL5 is still targeted to shaft and ankle links,
491 unranked stereocilia, and the kinocilium in P0-P3 inner and outer hair cells from both wild type and
492 *Pcdh15*$^{-/-}$ mutant mice (Mahendrasingam et al., 2017). Whether the kinocilial localization would
493 remain in mature cochlear hair cells is not known because the kinocilia degenerate by P8 in mice and
494 detailed LHFPL5 localization in vestibular hair cells (which retain their kinocilium) has not been
495 reported.

496 Zebrafish hair cells retain a kinocilium throughout their life, thus providing a different context in which
497 to examine Lhfpl5 localization. In wild type hair cells, GFP-Lhfpl5a is present at the tips of the shorter
498 ranked stereocilia, but the most robust signal is detected in the tallest stereocilia adjacent to the
499 kinocilium. In *pcdh15a* mutants, only this "kinocilial link"-like signal remains in the hair bundle. This
500 result is similar to the LHFPL5 localization reported at the tips of the tallest stereocilia of P3 cochlear
501 hair cells from wild type mice, a region where LHFPL5 would presumably not be associated with either
502 PCDH15 or the TMCs (Mahendrasingam et al., 2017). Since the kinocilium does not degenerate in
503 zebrafish hair cells, our results suggest that Lhfpl5a is normally targeted to these kinocilial links in
504 wild type cells and that its retention at this site does not require Pcdh15a. Thus, there are PCDH15-
505 dependent and PCDH15-independent mechanisms of LHFPL5 localization in both mouse and
506 zebrafish hair cells. These results suggest that LHFPL5 performs as-of-yet uncharacterized PCDH15-
507 independent functions as well.

508 Cdh23 is thought to form part of the linkages between the kinocilium and adjacent stereocilia, and
509 therefore may play a role in retaining Lhfpl5a at these sites. Consistent with this hypothesis, *cdh23*
510 mutants do not exhibit GFP-Lhfpl5a accumulation in stereocilia. Instead, GFP-Lhfpl5a is diffusely
511 distributed throughout the kinocilium. These data suggest that normal Lhfpl5a localization requires
512 both Pcdh15a and Cdh23 function, albeit in distinct ways. This result differs from previous reports
513 which found that Lhfpl5 still localized to the tips of stereocilia in CDH23-deficient cochlear hair cells

This is a provisional file, not the final typeset article

514 of mice. The same study also could not detect a biochemical interaction between Lhfpl5 and CDH23
515 via co-IP in heterologous cells (Xiong et al., 2012). Given these contrasting results for mouse and
516 zebrafish hair cells, it seems that the requirement for Cdh23 in the localization of LHFPL5 is not a
517 universal one.

518 Given the available biochemical evidence, it is possible that the association between Lhfpl5a and
519 Cdh23 is indirect through an as-of-yet unidentified protein or protein complex. Based on the defects in
520 GFP-Lhfpl5a localization in *myo7aa* mutants, Myo7aa is a candidate member of this uncharacterized
521 protein complex. Taken together, these results highlight the fact that, although all sensory hair cells
522 share many core genetic and biochemical features, there are important details that differ between the
523 various types of hair cells and between vertebrate species. Analyzing these differences will allow for
524 a more comprehensive understanding of vertebrate hair cell function and the underlying principles of
525 mechanotransduction.

526 6 Conflict of Interest

527 The authors declare that the research was conducted in the absence of any commercial or financial
528 relationships that could be construed as a potential conflict of interest.

529 7 Author Contributions

530 TE and TN conceived and designed the study; TE, IVP, AV, and RC collected and analyzed the data,
531 TE wrote the manuscript with Methods sections contributed by IVP and AV and editorial input from
532 TN and IVP.

533 8 Funding

534 This study was supported by funding from the NIDCD (R01 DC013572 and DC013531 to T.N.) and
535 from East Carolina University's Division of Research, Economic Development and Engagement
536 (REDE), Thomas Harriot College of Arts and Science (THCAS), and Department of Biology (to T.E.)

537 9 Acknowledgments

538 We thank Eliot Smith for assistance with CRISPR-Cas9 knockout of *lhfpl5b*. We also thank Leah
539 Snyder, Matthew Esqueda, and members of the Erickson lab for their assistance with animal
540 husbandry.

541 10 References

542 Allendorf, F. W., and Thorgaard, G. H. (1984). "Tetraploidy and the Evolution of Salmonid Fishes,"
543 in *Evolutionary Genetics of Fishes* (Boston, MA: Springer US), 1–53. doi:10.1007/978-1-4684-
544 4652-4_1.

545 Beurg, M., Xiong, W., Zhao, B., Müller, U., and Fettiplace, R. (2015). Subunit determination of the
546 conductance of hair-cell mechanotransducer channels. *Proc. Natl. Acad. Sci.* 112, 1589–1594.
547 doi:10.1073/pnas.1420906112.

548 Blanco-Sanchez, B., Clement, A., Fierro, J., Washbourne, P., and Westerfield, M. (2014). Complexes
549 of Usher proteins preassemble at the endoplasmic reticulum and are required for trafficking and
550 ER homeostasis. *Dis. Model. Mech.* 7, 547–559. doi:10.1242/dmm.014068.

551 Boëda, B., El-Amraoui, A., Bahloul, A., Goodyear, R., Daviet, L., Blanchard, S., et al. (2002).
552 Myosin VIIa, harmonin and cadherin 23, three Usher I gene products that cooperate to shape the
553 sensory hair cell bundle. *EMBO J.* 21, 6689–99. doi:10.1093/emboj/cdf689.

554 Braasch, I., Gehrke, A. R., Smith, J. J., Kawasaki, K., Manousaki, T., Pasquier, J., et al. (2016). The
555 spotted gar genome illuminates vertebrate evolution and facilitates human-teleost comparisons.
556 *Nat. Genet.* 48, 427–437. doi:10.1038/ng.3526.

557 Chou, S.-W., Chen, Z., Zhu, S., Davis, R. W., Hu, J., Liu, L., et al. (2017). A molecular basis for
558 water motion detection by the mechanosensory lateral line of zebrafish. *Nat. Commun.* 8, 2234.
559 doi:10.1038/s41467-017-01604-2.

560 Cunningham, C. L., and Müller, U. (2019). Molecular Structure of the Hair Cell Mechanoelectrical
561 Transduction Complex. *Cold Spring Harb. Perspect. Med.* 9, a033167.
562 doi:10.1101/cshperspect.a033167.

563 Cunningham, C. L., Wu, Z., Jafari, A., Zhao, B., Schrode, K., Harkins-Perry, S., et al. (2017). The
564 murine catecholamine methyltransferase mTOMT is essential for mechanotransduction by
565 cochlear hair cells. *Elife* 6. doi:10.7554/eLife.24318.

566 Dereeper, A., Guignon, V., Blanc, G., Audic, S., Buffet, S., Chevenet, F., et al. (2008). Phylogeny.fr:
567 robust phylogenetic analysis for the non-specialist. *Nucleic Acids Res.* 36, W465–W469.
568 doi:10.1093/nar/gkn180.

569 Erickson, T., French, C. R., and Waskiewicz, A. J. (2010). Meis1 specifies positional information in
570 the retina and tectum to organize the zebrafish visual system. *Neural Dev.* 5, 22.
571 doi:10.1186/1749-8104-5-22.

572 Erickson, T., Morgan, C. P., Olt, J., Hardy, K., Busch-Nentwich, E., Maeda, R., et al. (2017).
573 Integration of Tmc1/2 into the mechanotransduction complex in zebrafish hair cells is regulated
574 by Transmembrane O-methyltransferase (Tomt). *Elife* 6. doi:10.7554/eLife.28474.

575 Ernest, S., Rauch, G.-J., Haffter, P., Geisler, R., Petit, C., and Nicolson, T. (2000). Mariner is
576 defective in myosin VIIA: a zebrafish model for human hereditary deafness. *Hum. Mol. Genet.*
577 9, 2189–2196. doi:10.1093/hmg/9.14.2189.

578 Gagnon, J. A., Valen, E., Thyme, S. B., Huang, P., Ahkmetova, L., Pauli, A., et al. (2014). Efficient
579 Mutagenesis by Cas9 Protein-Mediated Oligonucleotide Insertion and Large-Scale Assessment
580 of Single-Guide RNAs. *PLoS One* 9, e98186. doi:10.1371/journal.pone.0098186.

581 Ge, J., Elferich, J., Goehring, A., Zhao, H., Schuck, P., and Gouaux, E. (2018). Structure of mouse
582 protocadherin 15 of the stereocilia tip link in complex with LHFPL5. *Elife* 7.
583 doi:10.7554/eLife.38770.

584 Giese, A. P. J., Tang, Y.-Q., Sinha, G. P., Bowl, M. R., Goldring, A. C., Parker, A., et al. (2017).
585 CIB2 interacts with TMC1 and TMC2 and is essential for mechanotransduction in auditory hair
586 cells. *Nat. Commun.* 8, 43. doi:10.1038/s41467-017-00061-1.

587 Glasauer, S. M. K., and Neuhauss, S. C. F. (2014). Whole-genome duplication in teleost fishes and
588 its evolutionary consequences. *Mol. Genet. Genomics* 289, 1045–1060. doi:10.1007/s00438-

This is a provisional file, not the final typeset article

589 014-0889-2.

590 Gleason, M. R., Nagiel, A., Jamet, S., Vologodskaia, M., López-Schier, H., and Hudspeth, A. J.
591 (2009). The transmembrane inner ear (Tmie) protein is essential for normal hearing and balance
592 in the zebrafish. *Proc. Natl. Acad. Sci. U. S. A.* 106, 21347–52. doi:10.1073/pnas.0911632106.

593 Goodyear, R. J., Forge, A., Legan, P. K., and Richardson, G. P. (2010). Asymmetric distribution of
594 cadherin 23 and protocadherin 15 in the kinocilial links of avian sensory hair cells. *J. Comp.*
595 *Neurol.* 518, 4288–4297. doi:10.1002/cne.22456.

596 György, B., Sage, C., Indzhykulian, A. A., Scheffer, D. I., Brisson, A. R., Tan, S., et al. (2017).
597 Rescue of Hearing by Gene Delivery to Inner-Ear Hair Cells Using Exosome-Associated AAV.
598 *Mol. Ther.* 25, 379–391. doi:10.1016/j.ymthe.2016.12.010.

599 Kawashima, Y., Géléoc, G. S. G., Kurima, K., Labay, V., Lelli, A., Asai, Y., et al. (2011).
600 Mechanotransduction in mouse inner ear hair cells requires transmembrane channel-like genes.
601 *J. Clin. Invest.* 121, 4796–809. doi:10.1172/JCI60405.

602 Kazmierczak, P., Sakaguchi, H., Tokita, J., Wilson-Kubalek, E. M., Milligan, R. A., Müller, U., et al.
603 (2007). Cadherin 23 and protocadherin 15 interact to form tip-link filaments in sensory hair
604 cells. *Nature* 449, 87–91. doi:10.1038/nature06091.

605 Lefevre, G., Michel, V., Weil, D., Lepelletier, L., Bizard, E., Wolfrum, U., et al. (2008). A core
606 cochlear phenotype in USH1 mouse mutants implicates fibrous links of the hair bundle in its
607 cohesion, orientation and differential growth. *Development* 135, 1427–1437.
608 doi:10.1242/dev.012922.

609 Li, X., Yu, X., Chen, X., Liu, Z., Wang, G., Li, C., et al. (2019). Localization of TMC1 and LHFPL5
610 in auditory hair cells in neonatal and adult mice. *FASEB J.* 33, 6838–6851.
611 doi:10.1096/fj.201802155RR.

612 Longo-Guess, C. M., Gagnon, L. H., Cook, S. A., Wu, J., Zheng, Q. Y., and Johnson, K. R. (2005). A
613 missense mutation in the previously undescribed gene Tmhs underlies deafness in hurry-scurry
614 (hscy) mice. *Proc. Natl. Acad. Sci.* 102, 7894–7899. doi:10.1073/pnas.0500760102.

615 Lu, Z., and DeSmidt, A. A. (2013). Early Development of Hearing in Zebrafish. *JARO J. Assoc. Res.*
616 *Otolaryngol.* 14, 509. doi:10.1007/S10162-013-0386-Z.

617 Lv, C., Stewart, W. J., Akanyeti, O., Frederick, C., Zhu, J., Santos-Sacchi, J., et al. (2016). Synaptic
618 Ribbons Require Ribeye for Electron Density, Proper Synaptic Localization, and Recruitment of
619 Calcium Channels. *Cell Rep.* 15, 2784–2795. doi:10.1016/j.celrep.2016.05.045.

620 Maeda, R., Kindt, K. S., Mo, W., Morgan, C. P., Erickson, T., Zhao, H., et al. (2014). Tip-link
621 protein protocadherin 15 interacts with transmembrane channel-like proteins TMC1 and TMC2.
622 *Proc. Natl. Acad. Sci. U. S. A.* 111, 12907–12. doi:10.1073/pnas.1402152111.

623 Maeda, R., Pacentine, I. V., Erickson, T., and Nicolson, T. (2017). Functional Analysis of the
624 Transmembrane and Cytoplasmic Domains of Pcdh15a in Zebrafish Hair Cells. *J. Neurosci.* 37,
625 3231–3245. doi:10.1523/JNEUROSCI.2216-16.2017.

626 Mahendrasingam, S., Fettiplace, R., Alagramam, K. N., Cross, E., and Furness, D. N. (2017).
627 Spatiotemporal changes in the distribution of LHFPL5 in mice cochlear hair bundles during
628 development and in the absence of PCDH15. *PLoS One* 12, e0185285.
629 doi:10.1371/journal.pone.0185285.

630 Morgan, C. P., Krey, J. F., Grati, M., Zhao, B., Fallen, S., Kannan-Sundhari, A., et al. (2016).
631 PDZD7-MYO7A complex identified in enriched stereocilia membranes. *Elife* 5.
632 doi:10.7554/eLife.18312.

633 Nicolson, T. (2017). The genetics of hair-cell function in zebrafish. *J. Neurogenet.* 31, 102–112.
634 doi:10.1080/01677063.2017.1342246.

635 Nicolson, T., Rüsch, A., Friedrich, R. W., Granato, M., Ruppersberg, J. P., and Nüsslein-Volhard, C.
636 (1998). Genetic analysis of vertebrate sensory hair cell mechanosensation: the zebrafish circler
637 mutants. *Neuron* 20, 271–83. doi:10.1016/S0896-6273(00)80455-9.

638 Obholzer, N., Swinburne, I. A., Schwab, E., Nechiporuk, A. V, Nicolson, T., and Megason, S. G.
639 (2012). Rapid positional cloning of zebrafish mutations by linkage and homozygosity mapping
640 using whole-genome sequencing. *Development* 139, 4280–4290. doi:10.1242/dev.083931.

641 Ohno, S. (1970). *Evolution by Gene Duplication*. Berlin, Heidelberg: Springer Berlin Heidelberg
642 doi:10.1007/978-3-642-86659-3.

643 Pacentine, I. V., and Nicolson, T. (2019). Subunits of the mechano-electrical transduction channel,
644 Tmc1/2b, require Tmie to localize in zebrafish sensory hair cells. *PLOS Genet.* 15, e1007635.
645 doi:10.1371/journal.pgen.1007635.

646 Pan, B., Akyuz, N., Liu, X.-P., Asai, Y., Nist-Lund, C., Kurima, K., et al. (2018). TMC1 Forms the
647 Pore of Mechanosensory Transduction Channels in Vertebrate Inner Ear Hair Cells. *Neuron* 99,
648 736-753.e6. doi:10.1016/j.neuron.2018.07.033.

649 Pan, B., Géléoc, G. S., Asai, Y., Horwitz, G. C., Kurima, K., Ishikawa, K., et al. (2013). TMC1 and
650 TMC2 Are Components of the Mechanotransduction Channel in Hair Cells of the Mammalian
651 Inner Ear. *Neuron* 79, 504–515. doi:10.1016/j.neuron.2013.06.019.

652 R Core Team (2019). R: A Language and Environment for Statistical Computing. Available at:
653 https://www.r-project.org/.

654 RStudio Team (2018). RStudio: Integrated Development Environment for R. Available at:
655 http://www.rstudio.com/.

656 Schneider, C. A., Rasband, W. S., and Eliceiri, K. W. (2012). NIH Image to ImageJ: 25 years of
657 image analysis. *Nat. Methods* 9, 671–5. Available at:
658 http://www.ncbi.nlm.nih.gov/pubmed/22930834 [Accessed January 13, 2019].

659 Seiler, C., Ben-David, O., Sidi, S., Hendrich, O., Rusch, A., Burnside, B., et al. (2004). Myosin VI is
660 required for structural integrity of the apical surface of sensory hair cells in zebrafish. *Dev. Biol.*
661 272, 328–38. doi:10.1016/j.ydbio.2004.05.004.

662 Seiler, C., Finger-Baier, K. C., Rinner, O., Makhankov, Y. V, Schwarz, H., Neuhauss, S. C. F., et al.

This is a provisional file, not the final typeset article

663 (2005). Duplicated genes with split functions: independent roles of protocadherin15 orthologues
664 in zebrafish hearing and vision. *Development* 132, 615–23. doi:10.1242/dev.01591.

665 Senften, M., Schwander, M., and Kazmierczak, P. (2006). Physical and functional interaction
666 between protocadherin 15 and myosin VIIa in mechanosensory hair cells. *J.* 26, 2060–2071.
667 doi:10.1523/JNEUROSCI.4251-05.2006.

668 Shabbir, M. I., Ahmed, Z. M., Khan, S. Y., Riazuddin, S., Waryah, A. M., Khan, S. N., et al. (2006).
669 Mutations of human TMHS cause recessively inherited non-syndromic hearing loss. *J. Med.*
670 *Genet.* 43, 634–40. doi:10.1136/jmg.2005.039834.

671 Sheets, L., Trapani, J. G., Mo, W., Obholzer, N., and Nicolson, T. (2011). Ribeye is required for
672 presynaptic CaV1.3a channel localization and afferent innervation of sensory hair cells.
673 *Development* 138, 1309–1319. doi:10.1242/dev.059451.

674 Sidi, S., Busch-Nentwich, E., Friedrich, R., Schoenberger, U., and Nicolson, T. (2004). gemini
675 encodes a zebrafish L-type calcium channel that localizes at sensory hair cell ribbon synapses. *J.*
676 *Neurosci.* 24, 4213–4223. doi:10.1523/JNEUROSCI.0223-04.2004.

677 Siemens, J., Lillo, C., Dumont, R. A., Reynolds, A., Williams, D. S., Gillespie, P. G., et al. (2004).
678 Cadherin 23 is a component of the tip link in hair-cell stereocilia. *Nature* 428, 950–955.
679 doi:10.1038/nature02483.

680 Singh, P. P., and Isambert, H. (2019). OHNOLOGS v2: a comprehensive resource for the genes
681 retained from whole genome duplication in vertebrates. *Nucleic Acids Res.*
682 doi:10.1093/nar/gkz909.

683 Söllner, C., Rauch, G.-J., Siemens, J., Geisler, R., Schuster, S. C., Müller, U., et al. (2004). Mutations
684 in cadherin 23 affect tip links in zebrafish sensory hair cells. *Nature* 428, 955–959.
685 doi:10.1038/nature02484.

686 Thisse, C., and Thisse, B. (2008). High-resolution in situ hybridization to whole-mount zebrafish
687 embryos. *Nat. Protoc.* 3, 59–69. doi:10.1038/nprot.2007.514.

688 Westerfield, M. (2000). *The zebrafish book. A guide for the laboratory use of zebrafish (Danio*
689 *rerio).* 4th ed. Eugene OR: University of Oregon Available at:
690 http://zfin.org/zf_info/zfbook/zfbk.html.

691 Wickham, H. (2016). *ggplot2: Elegant Graphics for Data Analysis*. Springer-Verlag New York
692 Available at: https://ggplot2.tidyverse.org.

693 Wolfe, K. (2000). Robustness—it's not where you think it is. *Nat. Genet.* 25, 3–4.
694 doi:10.1038/75560.

695 Xiong, W., Grillet, N., Elledge, H. M., Wagner, T. F. J., Zhao, B., Johnson, K. R., et al. (2012).
696 TMHS is an integral component of the mechanotransduction machinery of cochlear hair cells.
697 *Cell* 151, 1283–95. doi:10.1016/j.cell.2012.10.041.

698 Yao, Q., DeSmidt, A. A., Tekin, M., Liu, X., and Lu, Z. (2016). Hearing Assessment in Zebrafish
699 During the First Week Postfertilization. *Zebrafish* 13, 79. doi:10.1089/ZEB.2015.1166.

700 Zhao, B., Wu, Z., Grillet, N., Yan, L., Xiong, W., Harkins-Perry, S., et al. (2014). TMIE Is an
701 Essential Component of the Mechanotransduction Machinery of Cochlear Hair Cells. *Neuron*
702 84, 954–967. doi:10.1016/j.neuron.2014.10.041.

703 Zou, J., Chen, Q., Almishaal, A., Mathur, P. D., Zheng, T., Tian, C., et al. (2017). The roles of USH1
704 proteins and PDZ domain-containing USH proteins in USH2 complex integrity in cochlear hair
705 cells. *Hum. Mol. Genet.* 26, 624–636. doi:10.1093/hmg/ddw421.

706

This is a provisional file, not the final typeset article

11 Figures

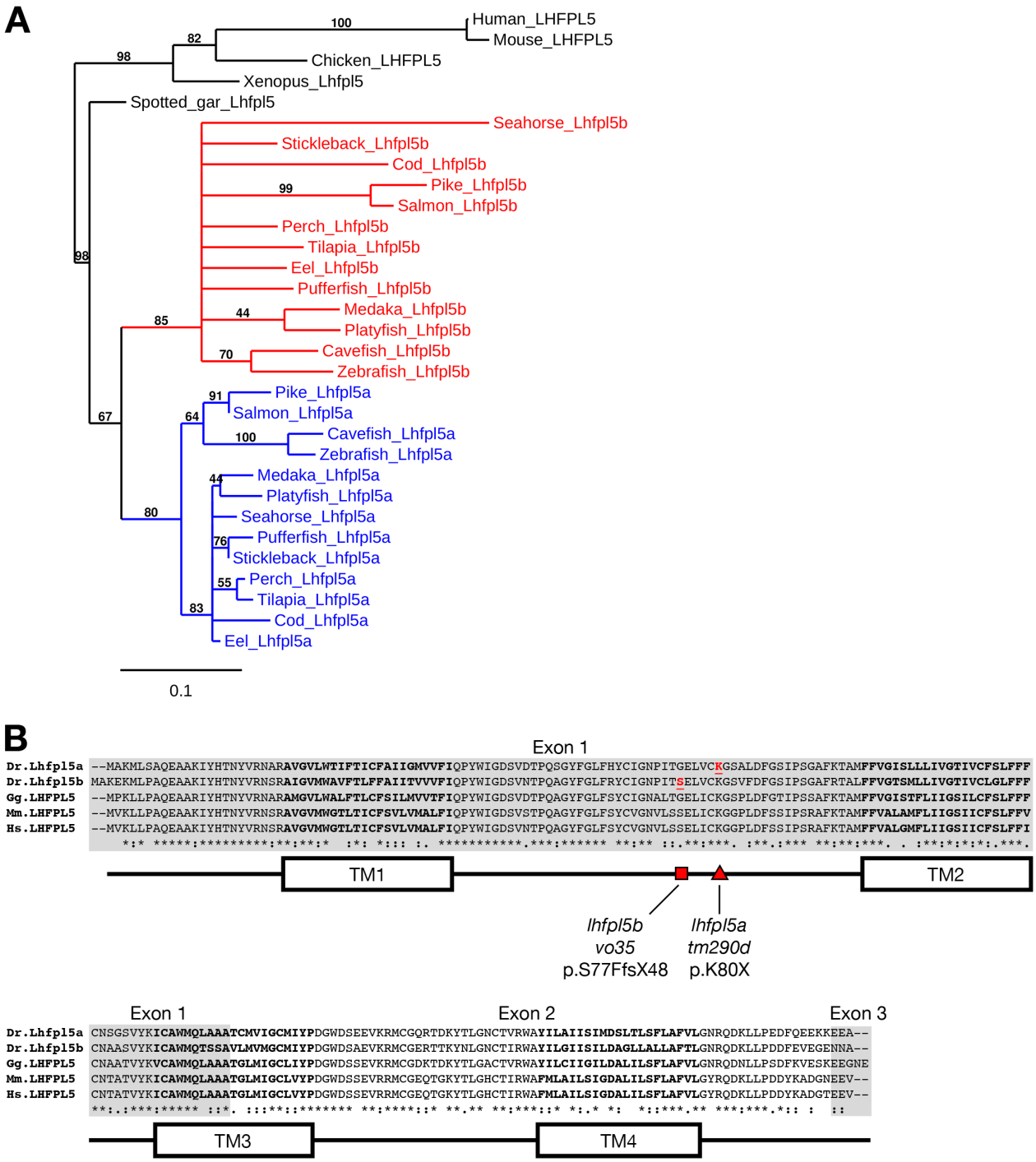

Figure 1. Duplicated *lhfpl5* genes in teleost fish. (**A**) Phylogenic tree of representative teleost and vertebrate Lhfpl5 protein sequences. See Supplemental Table 1 for species' names and protein accession numbers. (**B**) Sequence alignment of Lhfpl5 proteins from zebrafish (*Danio rerio*, Dr), chicken (*Gallus gallus*, Gg), mouse (*Mus musculus*, Mm), and humans (*Homo sapiens*, Hs). Regions of the proteins coded for by exons 1 and 3 are shaded grey. Locations of the transmembrane (TM) helices 1-4 are shown in the linear protein structure diagram. The *lhfpl5a*^{tm290d} and *lhfpl5b*^{vo35} mutations are indicated by the red triangle and red square, respectively.

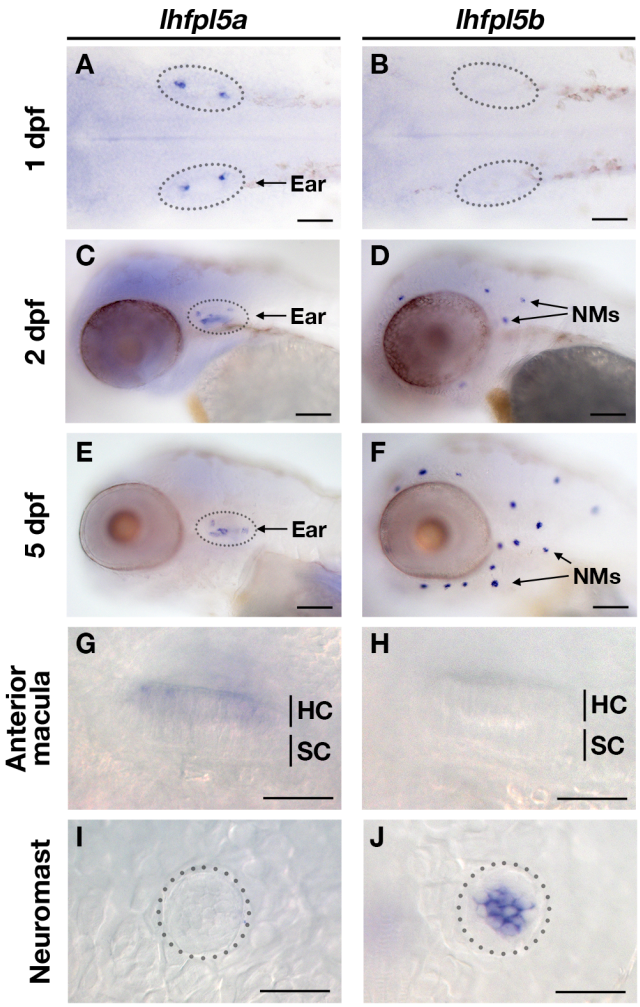

716

717 **Figure 2.** Zebrafish *lhfpl5a* and *lhfpl5b* genes are expressed in distinct populations of sensory hair
718 cells. Whole mount mRNA *in situ* hybridization for *lhfpl5a* (**A, C, E, G, I**) and *lhfpl5b* (**B, D, F, H, J**)
719 at 1, 2, and 5 days post-fertilization (dpf). Panels G - J are details from 5 dpf larvae. Abbreviations:
720 NMs = neuromasts, HC = hair cell, SC = support cell. Scale bars: A, B = 50 µm; C - F = 100 µm; G -
721 J = 25 µm.

722

This is a provisional file, not the final typeset article

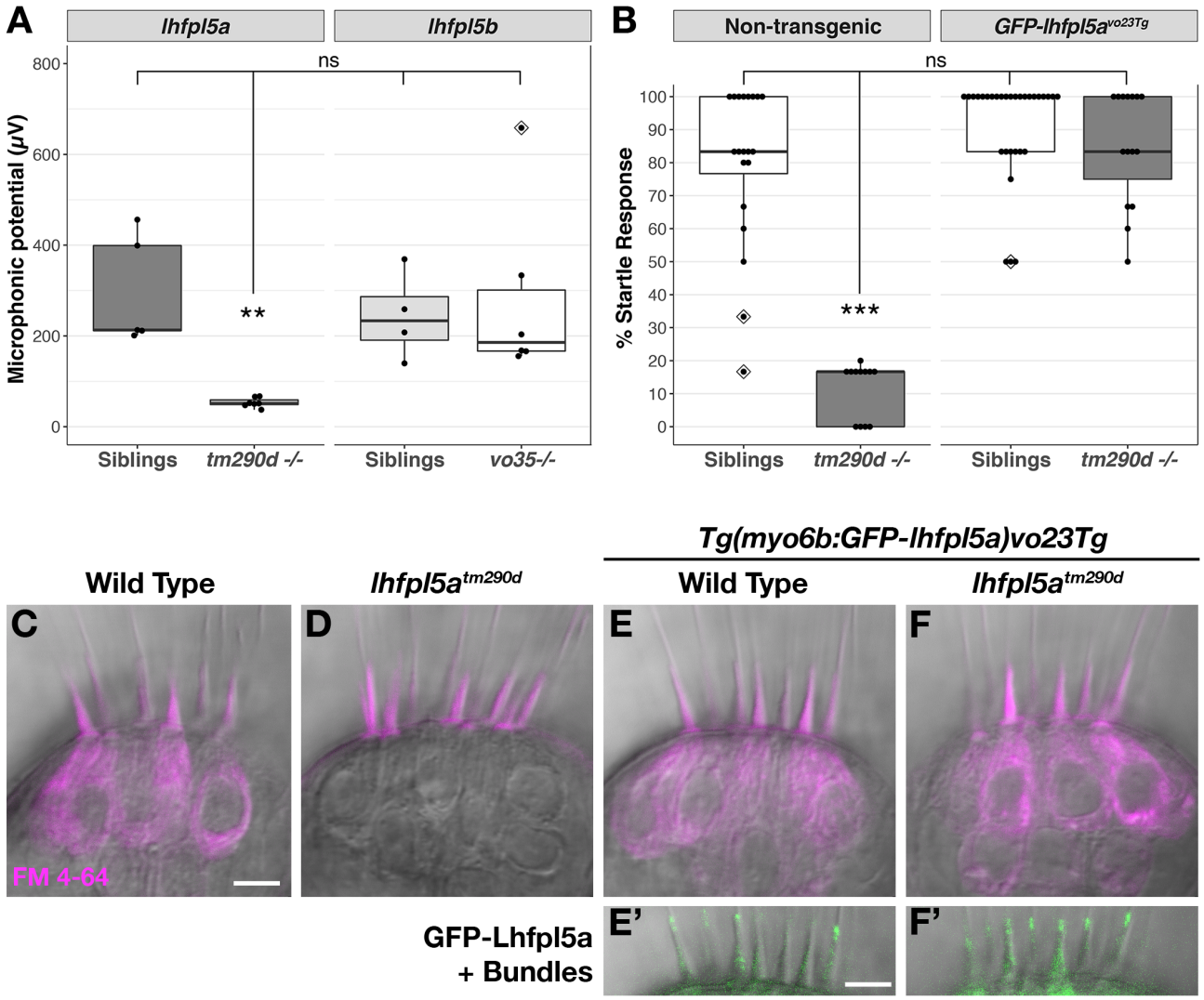

723

724 **Figure 3.** *lhfpl5a* is required for auditory and vestibular hair cell function. (**A**) Boxplot showing the
725 first peak amplitude (µV) of microphonic recordings from the inner ear of 3 dpf wild type, *lhfpl5a*^{tm290d},
726 and *lhfpl5b*^{vo35} larvae. The boxes cover the inter-quartile range (IQR), and the whiskers represent the
727 minimum and maximum datapoints within 1.5 times the IQR. Values from individual larvae are
728 indicated by the black dots and outliers indicated by a diamond. Asterisks indicate $p < 0.01$ (**) by
729 Welch's t-test. ns = not significant. (**B**) Boxplot of the acoustic startle response in 6 dpf wild type and
730 *lhfpl5a*^{tm290d} mutants, with or without the *GFP-lhfpl5a vo23Tg* transgene. Values from individual
731 larvae are indicated by the black dots and outliers indicated by a diamond. Asterisks indicate $p < 0.001$
732 (***) by Welch's t-test. ns = not significant. (**C-F'**) FM 4-64 dye labeling assay for MET channel
733 activity of inner ear hair cells from 6 dpf larvae (C - Wild type (+/+ *or* +/-), D - *lhfpl5a*^{tm290d} mutants,
734 E - Wild type *GFP-lhfpl5a vo23Tg*, F - GFP-*lhfpl5a vo23Tg; lhfpl5a*^{tm290}). E' and F' are images of
735 GFP-Lhfpl5a protein in the bundle of the hair cells shown above in panels E and F. n = 2, 3, 12, and 4
736 for the genotypes in panels C-F, respectively. Scale bars = 5 µm and apply to all images.

737

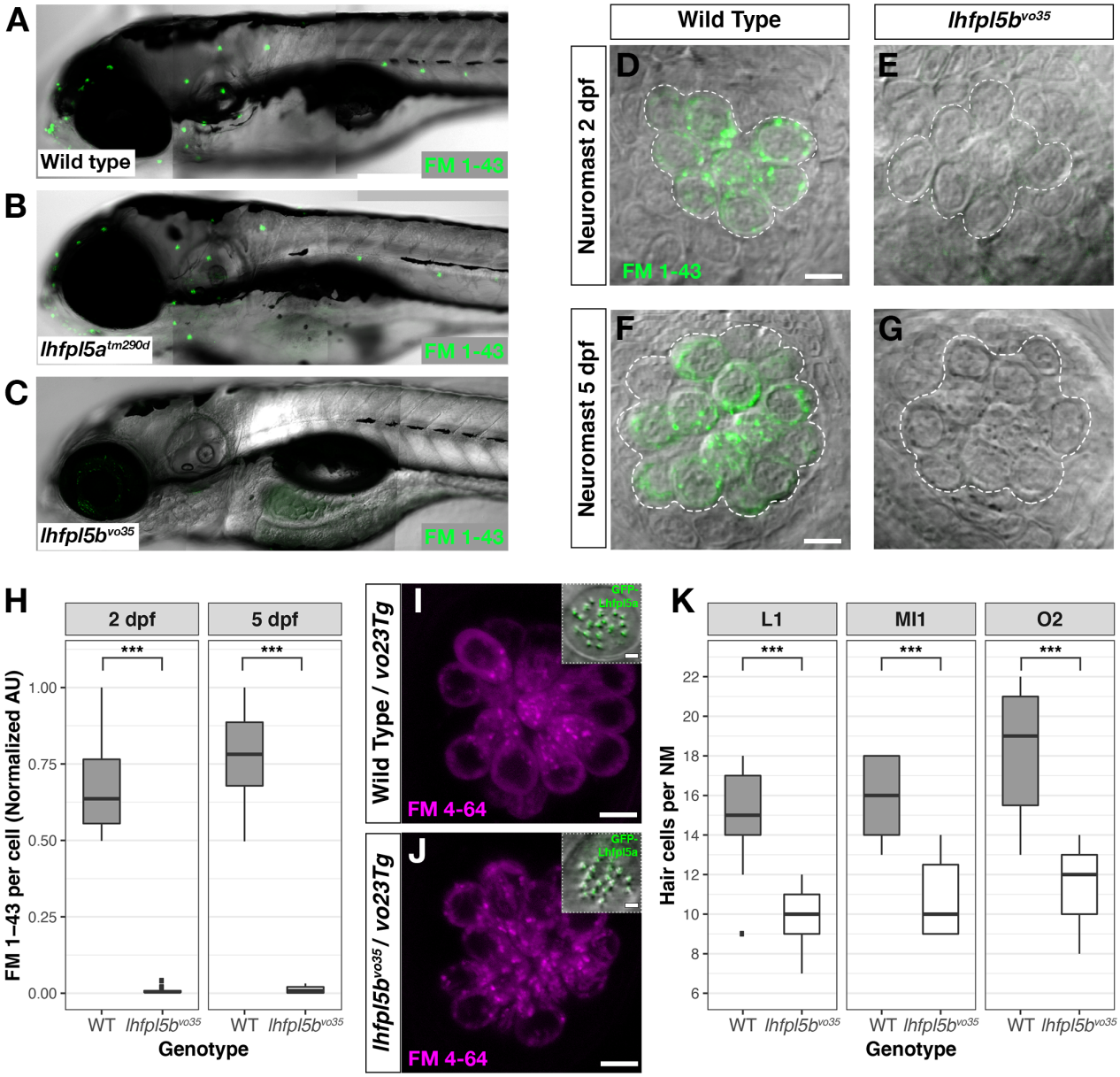

Figure 4. *lhfpl5b* is required for lateral line hair cell function. (**A-C**) Representative images of 5 dpf zebrafish larvae (A - Wild type; B - *lhfpl5a*^{tm290d}; C - *lhfpl5b*^{vo35}) labeled with the MET channel-permeant dye FM 1-43. (**D-G**) Representative images of individual neuromasts from 2 dpf and 5 dpf wild type and *lhfpl5b*^{vo35} larvae labeled with FM 1-43. Dashed lines outline the cluster of hair cells in each neuromast. (**H**) Quantification of normalized FM 1-43 fluorescence intensity per hair cell of 2 dpf and 5 dpf neuromasts (n = 10 WT, 14 *lhfpl5b*^{vo35} NMs at 2 dpf; n = 6 WT, 13 *lhfpl5b*^{vo35} NMs each genotype at 5 dpf). The box plots cover the inter-quartile range (IQR), and the whiskers represent the minimum and maximum datapoints within 1.5 times the IQR. Asterisks indicate $p < 0.001$ (***) by Welch's t-test. (**I, J**) Rescue of FM dye labeling in *lhfpl5b*^{vo35} mutants (n = 7) by the *GFP-lhfpl5a* (*vo23Tg*) transgene. The GFP-Lhfpl5a bundle and FM 4–64 images are from the same NM for each genotype. (**K**) Quantification of hair cell number in L1, MI1, and O2 neuromasts from 5 dpf *lhfpl5b*^{vo35} mutants (n = 11) and wild-type siblings (n = 11). The box plots are the same as in H. Asterisks indicate $p < 0.001$ (***) by Welch's t-test. Scale bars = 5 µm, applies to panels D-G, I, J; 2 µm in I, J insets).

This is a provisional file, not the final typeset article

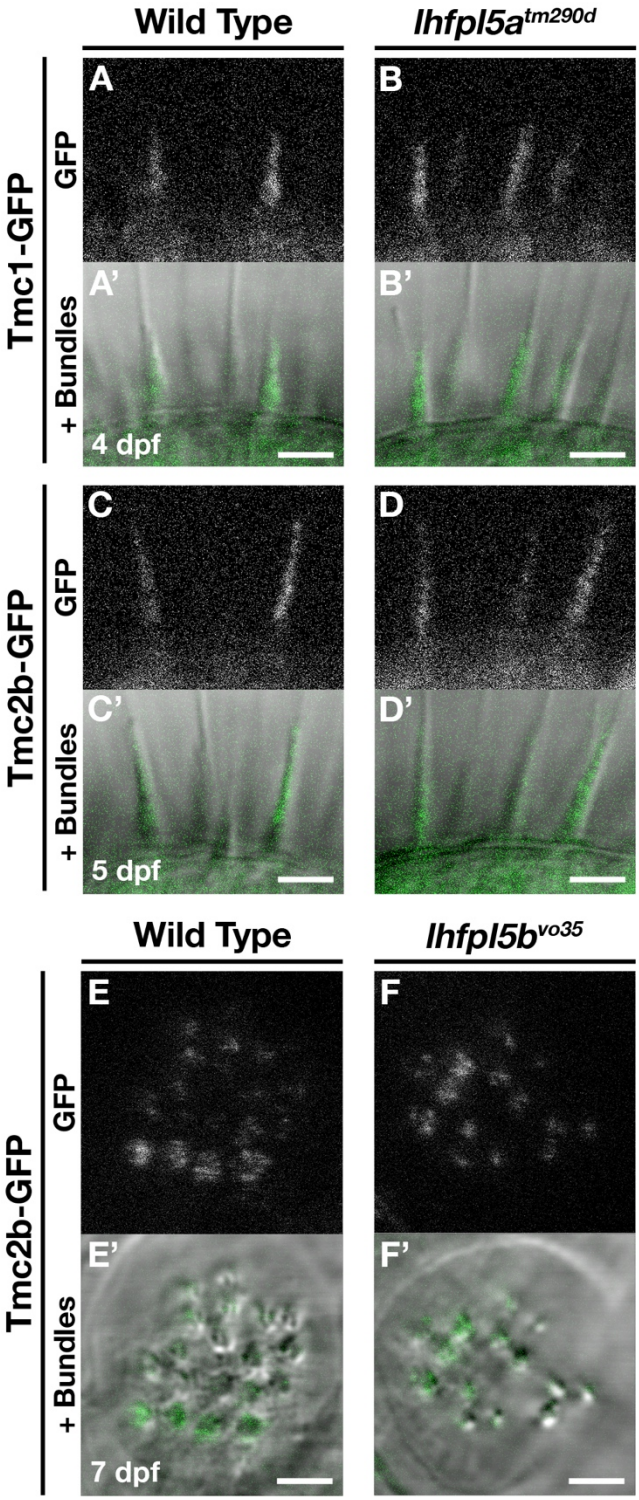

752

753 **Figure 5.** Tmc proteins do not require Lhfpl5a or Lhfpl5b for localization to the stereocilia of zebrafish
754 hair cells. (**A – D'**) Representative images of Tmc1-GFP (*vo27Tg*) or Tmc2b-GFP (*vo28Tg*) in the
755 lateral cristae of wild type (**A, A', C, C'**) and *lhfpl5a*^{tm290d} (**B, B', D, D'**) larvae. The GFP-only channel
756 is shown in panels A - D and overlaid with a light image of the bundles in A' - D'. (**E – F'**)
757 Representative images of Tmc2b-GFP (*vo28Tg*) in the neuromasts of wild type (**E, E'**) and *lhfpl5b*^{vo35}
758 (**F, F'**) larvae. The GFP-only channel is shown in panels E and F and overlaid with a light image of
759 the bundles in E' and F'. Scale bars = 3 µm in all panels.

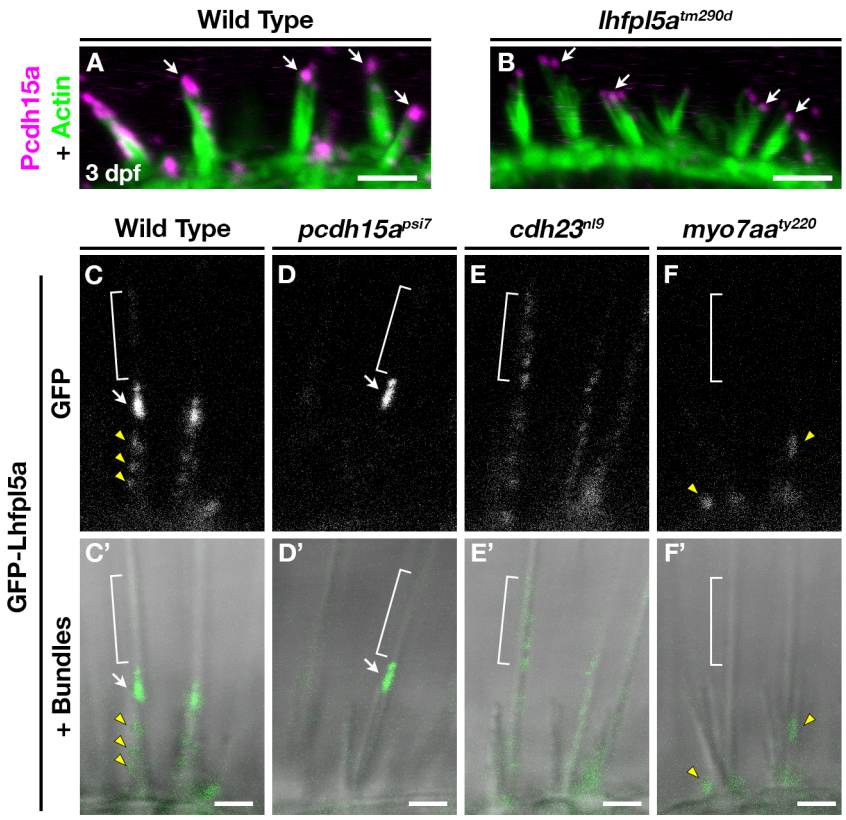

Figure 6. Lhfpl5a requires MET complex proteins Pcdh15a, Cdh23, and Myo7a for normal localization in the stereocilia of zebrafish hair cells. (**A, B**) Immunostain of Pcdh15a (magenta) in the lateral cristae of wild type and *lhfpl5a*^{tm290d} mutants at 3 dpf. Phalloidin-stained actin of the hair bundle is shown in green. Arrows indicate areas of Pcdh15a accumulation. (**C-F'**) Representative images of GFP-Lhfpl5a (*vo23Tg*) in the lateral cristae hair bundles of wild type (**C, C'**) and *pcdh15a*^{psi7} (**D, D'**), *cdh23*^{nl9} (**E, E'**), and *myo7aa*^{ty220} (**F, F'**) mutants. White arrows indicate GFP signal in the presumptive kinocilial linkages, yellow arrow heads indicate GFP signal in the stereocilia or the base of the hair bundle, and brackets indicate GFP signal in the kinocilium. Scale bars = 3 µm in A, B; 2 µm in C-F'.

This is a provisional file, not the final typeset article

769 **Supplemental Table 1.** Lhfpl5 proteins used to construct the phylogenetic tree in Figure 1A.

Common name	Species	Phylogenetic Order	Gene name	Accession number
Seahorse	*Hippocampus comes*	Syngnathiformes	*lhfpl5a*	XP_019736131.1
			lhfpl5b	XP_019716386.1
Salmon (Atlantic)	*Salmo salar*	Salmoniformes	*lhfpl5a*	XP_014021466.1
			lhfpl5b	XP_014002848.1
Pufferfish	*Takifugu rubripes*	Tetraodontiformes	*lhfpl5a*	ENSTRUP00000020283.2
			lhfpl5b	ENSTRUP00000041734.2
Platyfish	*Xiphophorus maculatus*	Cyprinodontiformes	*lhfpl5a*	ENSXMAP00000020967.1
			lhfpl5b	ENSXMAP00000010306.1
Medaka	*Oryzias latipes*	Beloniformes	*lhfpl5a*	ENSORLP00000042616.1
			lhfpl5b	ENSORLP00000008018.2
Zebrafish	*Danio rerio*	Cypriniformes	*lhfpl5a*	ENSDARP00000066188.3
			lhfpl5b	ENSDARP00000073423.4
Cavefish (Blind)	*Astyanax mexicanus*	Characiformes	*lhfpl5a*	ENSAMXP00000035004.1
			lhfpl5b	ENSAMXP00000007271.2
Stickleback (3-spine)	*Gasterosteus aculeatus*	Gasterosteiformes	*lhfpl5a*	ENSGACP00000010149.1
			lhfpl5b	ENSGACP00000010766.1
Tilapia	*Oreochromis niloticus*	Cichliformes	*lhfpl5a*	ENSONIP00000024352.1
			lhfpl5b	ENSONIP00000014897.1
Perch (Climbing)	*Anabas testudineus*	Perciformes	*lhfpl5a*	ENSATEP00000035217.1
			lhfpl5b	ENSATEP00000029406.1
Eel (Zig-zag)	*Mastacembelus armatus*	Synbranchiformes	*lhfpl5a*	ENSMAMP00000013383.1
			lhfpl5b	ENSMAMP00000016042.1
Cod	*Gadus morhua*	Gadiformes	*lhfpl5a*	ENSGMOP00000012109.1
			lhfpl5b	ENSGMOP00000016613.1
Pike (Northern)	*Esox lucius*	Esociformes	*lhfpl5a*	ENSELUP00000020567.1
			lhfpl5b	ENSELUP00000014071.1
Spotted gar	*Lepisosteus oculatus*	Lepisosteiformes	*lhfpl5*	ENSLOCP00000013703.1
Xenopus	*Xenopus tropicalis*	Anura	*lhfpl5*	ENSXETP00000058779.1
Chicken	*Gallus gallus*	Galliformes	*lhfpl5*	ENSGALP00000053562.1
Mouse	*Mus musculus*	Rodentia	*lhfpl5*	ENSMUSP00000156557.1
Human	*Homo sapiens*	Primates	*lhfpl5*	ENSP00000493955.1

770

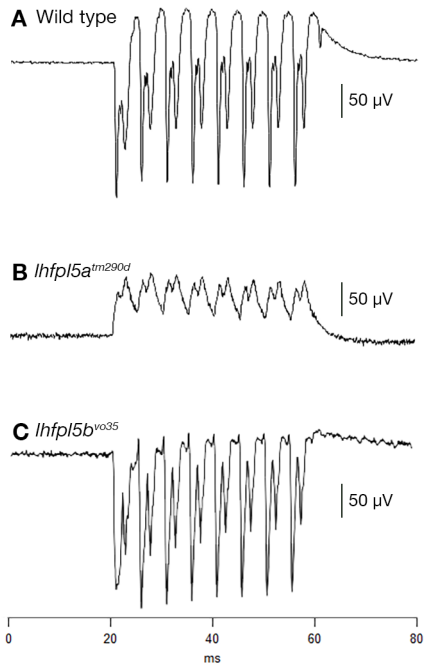

D

Genotype	n	Mean	Median	Std. Dev.	25-75 pctl.
Siblings (*tm290d*)	5	296.20	213.02	121.76	211.57 - 399.02
lhfpl5a^{tm290d}	7	53.06	51.14	10.48	48.83 - 59.05
Siblings (*vo35*)	4	243.84	233.35	96.74	190.78 - 286.41
lhfpl5b^{vo35}	6	280.86	185.64	196.47	166.67 - 301.01

Supplemental Figure 1. Representative microphonic traces from the inner ears of 3 day-old wild type (**A**), *lhfpl5a*^{tm290d} (**B**), and *lhfpl5b*^{vo35} (**C**) larvae. **D** – Table of the n-values, mean, median, standard deviation, and 25 - 75 percentile values for the first peak microphonic values graphed in Figure 3A.

This is a provisional file, not the final typeset article

776

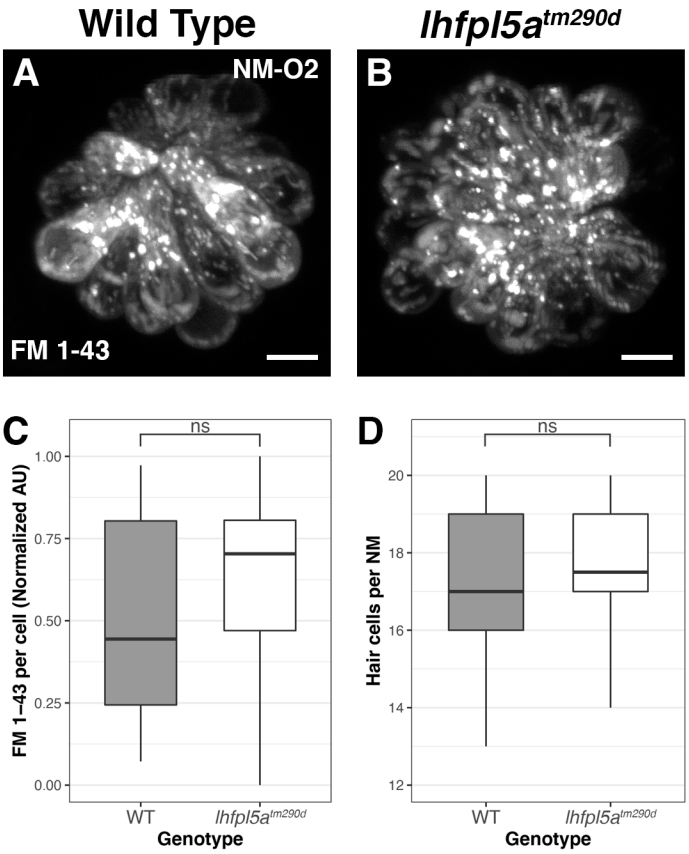

777

778 **Supplemental Figure 2.** Comparison of basal MET channel activity in neuromasts from wild type and
779 *lhfpl5a*^{tm290d} mutant larvae. (**A, B**) Representative images of FM 1-43 fluorescence in lateral line
780 neuromasts from wild type (A) and *lhfpl5a*^{tm290d} (B) mutants at 5 dpf. (**C**) Quantification of normalized
781 FM 1-43 fluorescence intensity per hair cell in 5 dpf neuromasts (n = 6 WT, 6 *lhfpl5a*^{tm290d} larvae, 3
782 NMs per larvae). The box plots cover the inter-quartile range (IQR), and the whiskers represent the
783 minimum and maximum datapoints within 1.5 times the IQR. p = 0.2229; ns = not significant. (**D**)
784 Quantification of hair cell number in neuromasts from 5 dpf *lhfpl5a*^{tm290d} mutants and wild-type
785 siblings, as determined by counting FM-positive hair cells. The same larvae and neuromasts were used
786 as in C. p = 0.5828; ns = not significant by Welch's t-test.

787

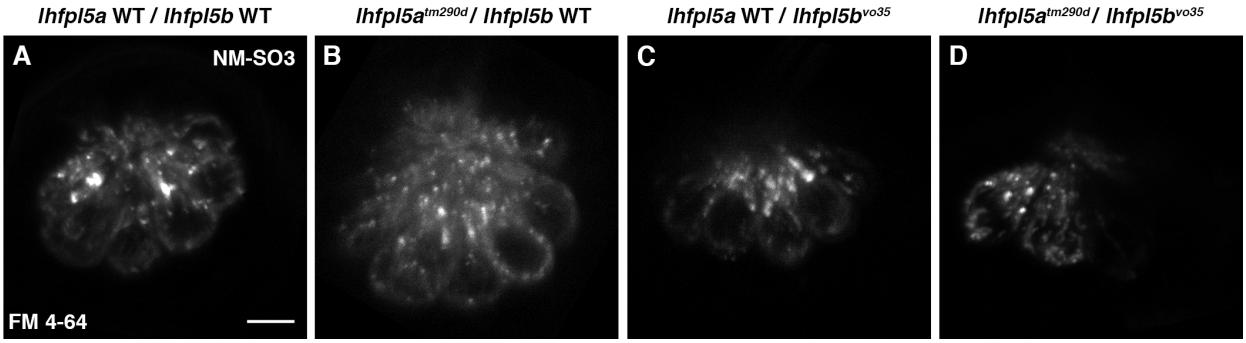

788

789 **Supplemental Figure 3.** Examples of residual basal MET channel activity in the SO3 neuromast hair
790 cells of *lhfpl5b*^{vo35} mutants and *lhfpl5a*^{tm290d}; *lhfpl5b*^{vo35} double mutants. FM 4-64 labeled SO3
791 neuromasts from wild type (**A**), *lhfpl5a*^{tm290d} (**B**), *lhfpl5b*^{vo35} (**C**), and *lhfpl5a*^{tm290d}; *lhfpl5b*^{vo35} (**D**)
792 larvae at 5 dpf. Scale bar = 5 µm, applies to all panels.

793

794

This is a provisional file, not the final typeset article

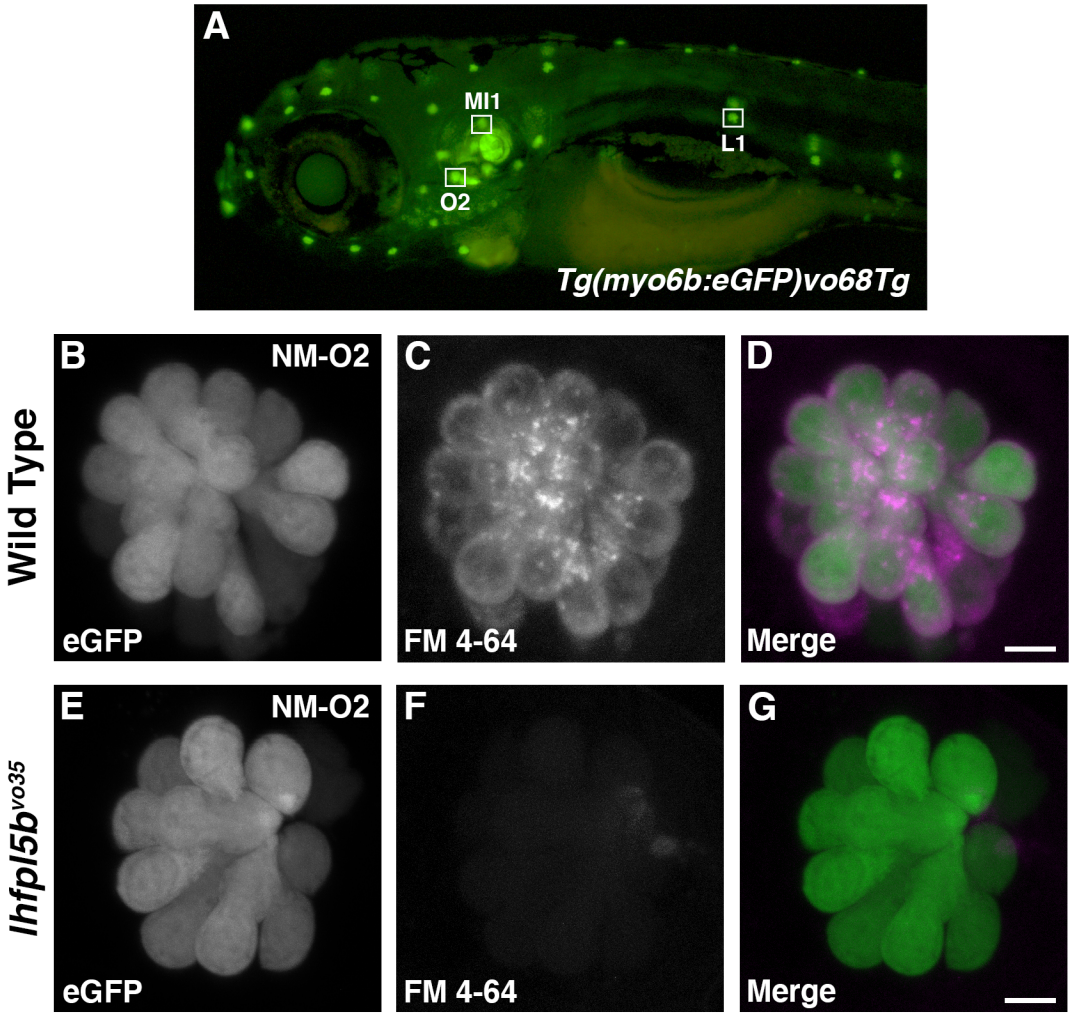

Supplemental Figure 4. (**A**) *Tg(myo6b:GFP)vo68Tg* larvae at 5 dpf. The neuromasts used for hair cell counting are labeled. (**B – G**) Representative images of GFP and FM 4-64-labeled hair cells in 5 dpf wild type and *lhfpl5b*^{vo35} mutant *Tg(myo6b:GFP)vo68Tg* larvae. These images are from larvae that make up part of the data set quantified in Figure 4K. Scale bars = 5 µm.

815

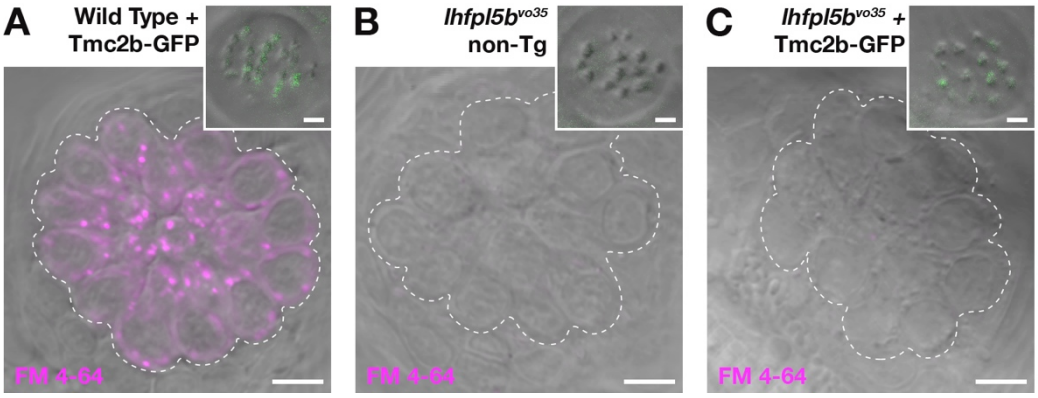

816

817 **Supplemental Figure 5.** Bundle-localized Tmc2b-GFP does not restore basal MET channel activity
818 to neuromast hair cells of *lhfpl5b*^{vo35} mutants. (**A-C**) Representative images of neuromasts labeled with
819 FM 4-64 from wild type Tmc2b-GFP *vo28Tg* (**A**), non-transgenic *lhfpl5b*^{vo35} (**B**), and *vo28Tg*;
820 *lhfpl5b*^{vo35} (**C**) larvae at 7 dpf. Dashed lines outline the cluster of hair cells in each neuromast. Insets
821 show the neuromast hair bundles from the same neuromast in the main panel. Scale bars = 5 µm in A-
822 C; 2 µm for the bundle insets.

823

824

This is a provisional file, not the final typeset article

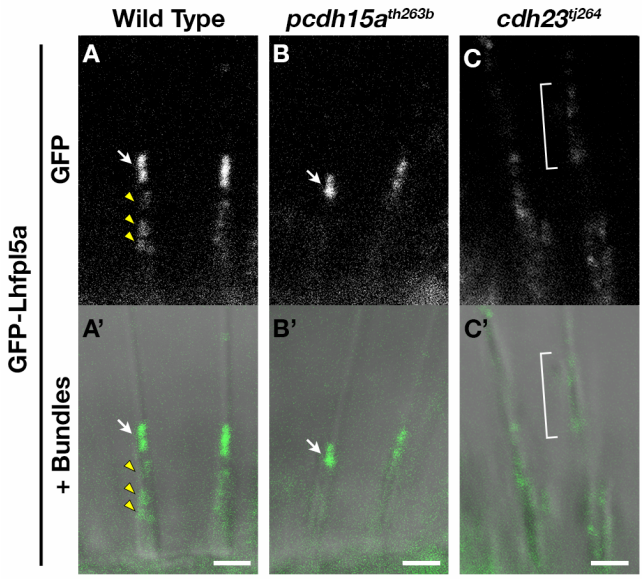

Supplemental Figure 6. Mislocalization of GFP-Lhfpl5a in different mutant alleles of *pcdh15a* and *cdh23* as shown in Figure 6. Representative images of GFP-Lhfpl5a (*vo23Tg*) in the lateral cristae hair bundles of wild type (**A, A'**) and *pcdh15a*^{th263b} (**B, B'**), and *cdh23*^{tj264} (**C, C'**) mutants. The GFP-only channel is shown in panels A - C and overlaid with a light image of the bundles in A' - C'. White arrows indicate GFP signal in the presumptive kinocilial linkages, yellow arrow heads indicate GFP signal in the stereocilia, and brackets indicate GFP signal in the kinocilium. Scale bars = 2 µm in A-C'.